Light Emitting Diodes and Solid-State Lighting

E. Fred Schubert

Department of Electrical, Computer, and Systems Engineering

Department of Physics, Applied Physics, and Astronomy

Rensselaer Polytechnic Institute, Troy, NY 12180

Phone: 518-276-8775 Email: EFSchubert@rpi.edu Internet: www.LightEmittingDiodes.org

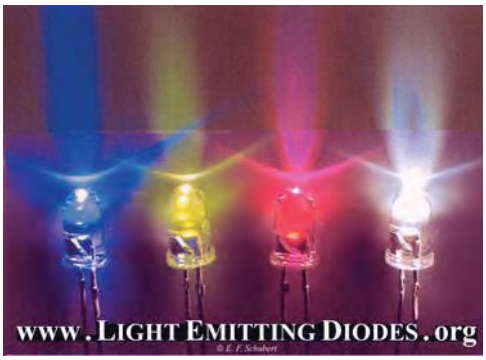

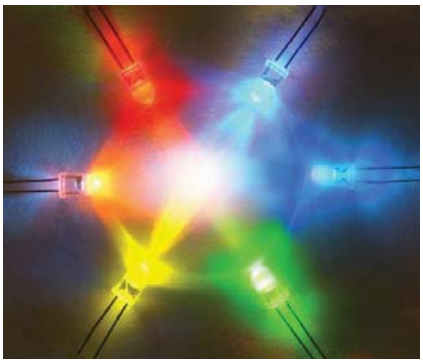

Solid-state lighting

- Inorganic devices:
  - Semiconductor plus phosphor illumination devices
  - All-semiconductor-based illumination devices
- Organic devices:
  - Remarkable successes in low-power devices (Active matrix OLED monitors, thin-film transistors, etc.)
  - Substantial effort is underway to demonstrate high-power devices
  - Anticipated manufacturing cost and luminance of organic devices are *orders of magnitude* different from inorganic devices

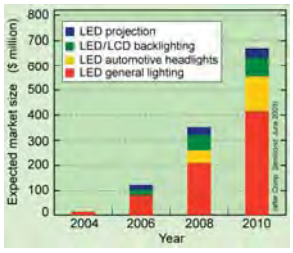

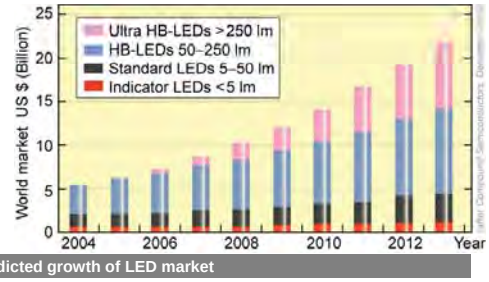

Predicted growth of LED market

OLED versus LED

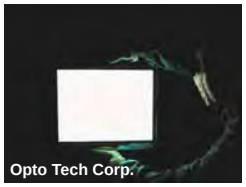

OLEDs are **area** sources
They do **do not blind**
Suitable for large-area sources

LEDs are **point** sources
They are **blindingly bright**
Suitable for imaging-optics applications

- Luminance of OLEDs: $10^2 – 10^4$ cd/m^2
- Luminance of LEDs: $10^6 – 10^7$ cd/m^2
- Luminance of OLEDs is about 4 orders of magnitude lower
- OLED manufacturing cost per unit area must be $10^4 \times$ lower

OLEDs	**LEDs**
Low-cost reel-to-reel manufacturing	Expensive epitaxial growth

Quantification of solid-state lighting benefits

- **Energy benefits**
  - 22 % of electricity used for lighting
  - LED-based lighting can be **20** × more efficient than incandescent and **5** × more efficient than fluorescent lighting
- **Environmental and economic benefits**
  - Reduction of **CO_2** emissions, a **global warming gas**
  - Reduction of **SO_2** emissions, **acid rain**
  - Reduction of **Hg** emissions by coal-burning power plants
  - Reduction of hazardous **Hg** in homes
- **Financial benefits**
  - Electrical energy cost reduction, but also savings resulting from less pollution, global warming

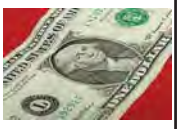

Quantification of benefits

Global benefits enabled by solid-state lighting technology over period of 10 years. First numeric value in each box represents annual US value.

The USA uses about ¼ of world's energy.

	Savings under "11% scenario"
Reduction in total energy consumption	43.01 × 10^{18} J × 11% × 4 × 10 = = 189.2 × 10^{18} J
Reduction in electrical energy consumption	457.8 TWh × 4 × 10 = = 18,310 TWh = 65.92 × 10^{18} J
Financial savings	45.78 × 10^{9} $ × 4 × 10 = = 1,831 × 10^{9} $
Reduction in CO_2 emission	267.0 Mt × 4 × 10 = 10.68 Gt
Reduction of crude-oil consumption (1 barrel = 159 liters)	24.07 × 10^{6} barrels × 4 × 10 = = 962.4 × 10^{6} barrels
Number of power plants not needed	70 × 4 = 280

(*) 1.0 PWh = 1000 TWh = 11.05 PBtu = 11.05 quadrillion Btu "=" 0.1731 Pg of C = 173.1 Mtons of C
1 kg of C "=" [(12 amu + 2 × 16 amu) / 12 amu] kg of CO_2 = 3.667 kg of CO_2

Schubert *et al.*, *Reports on Progress in Physics* **69**, 3069 (2006)

History of LEDs

- Henry Joseph Round (1881 – 1966)
- 1907: First observation of electroluminescence
- 1907: First LED
- LED was made of SiC, carborundum, an abrasive material

A Note on Carborundum.

To the Editors of Electrical World:

SIRS:—During an investigation of the unsymmetrical passage of current through a contact of carborundum and other substances a curious phenomenon was noted. On applying a potential of 10 volts between two points on a crystal of carborundum, the crystal gave out a yellowish light. Only one or two specimens could be found which gave a bright glow on such a low voltage, but with 110 volts a large number could be found to glow. In some crystals only edges gave the light and others gave instead of a yellow light green, orange or blue. In all cases tested the glow appears to come from the negative pole, a bright blue-green spark appearing at the positive pole. In a single crystal, if contact is made near the center with the negative pole, and the positive pole is put in contact at any other place, only one section of the crystal will glow and that the same section wherever the positive pole is placed.

There seems to be some connection between the above effect and the e.m.f. produced by a junction of carborundum and another conductor when heated by a direct or alternating current; but the connection may be only secondary as an obvious explanation of the e.m.f. effect is the thermoelectric one. The writer would be glad of references to any published account of an investigation of this or any allied phenomena.

NEW YORK, N. Y. H. J. ROUND.

Henry Joseph Round

Light-Emitting Diode – 1924 – SiC – Lossev

- Oleg Vladimirovich Lossev (1903 – 1942)
- Brilliant scientist who published first paper at the age of 20 years
- The Lossevs were noble family of a Russian Imperial Army officer
- Lossev made first detailed study of electroluminescence in SiC
- Lossev concluded that luminescence is no heat glow (incandescence)
- Lossev noted similarity to vacuum gas discharge

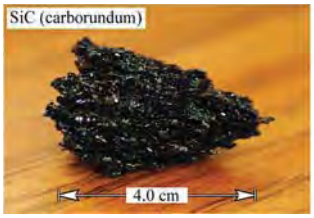

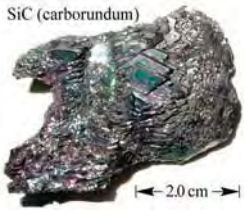

SiC – Carborundum

Oleg Vladimirovich Lossev

Light-Emitting Diode – 1924 – SiC – Lossev

- Oleg V. Lossev noted light emission for forward and reverse voltage
- Measurement period 1924 – 1928

First photograph of light emitted by SiC LED

(after O. V. Lossev, 1924)

SiC crystal

First photograph of LED

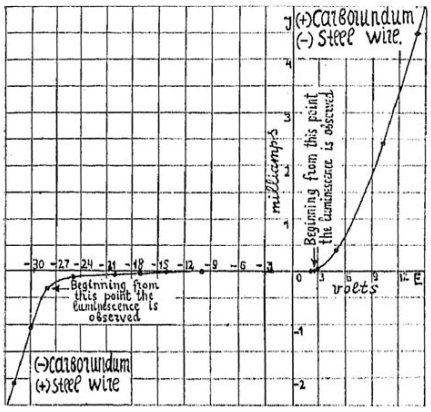

Lossev's I-V characteristic

Light emission in first LED

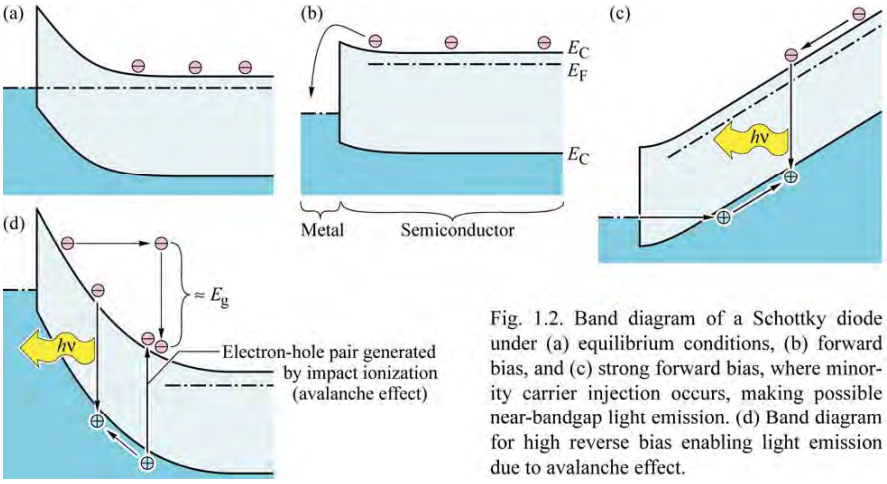

Fig. 1.2. Band diagram of a Schottky diode under (a) equilibrium conditions, (b) forward bias, and (c) strong forward bias, where minority carrier injection occurs, making possible near-bandgap light emission. (d) Band diagram for high reverse bias enabling light emission due to avalanche effect.

- First LED did not have pn junction!
- Light was generated by either minority carrier injection (forward) or avalanching (reverse bias)
- "Beginner's luck"

History of AlGaAs IR and red LEDs

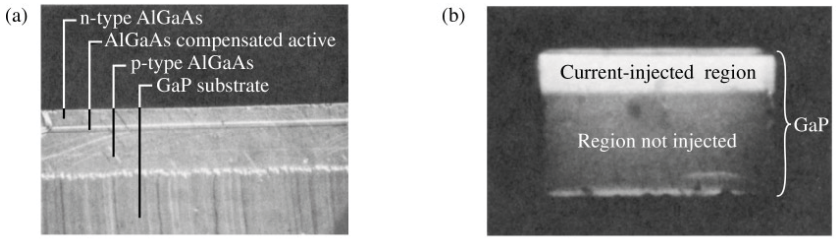

Fig. 1.3. (a) Cross section micrograph of a an AlGaAs LED grown on a transparent GaP substrate. (b) Electroluminescence originating from a current-injected region located under a stripe-shaped contact viewed through the transparent GaP substrate (after Woodall *et al.*, 1972).

- There is lattice mismatch between AlGaAs and GaAs
- Growth by liquid phase epitaxy (LPE)
- Growth technique to date: Organometallic vapor Phase epitaxy

One of the first application of LEDs

Fig. 1.4. This classic 1964 main-frame computer IBM System 360 used high-voltage gas-discharge lamps to indicate the status of the arithmetic unit. In later models, the lamps were replaced by LEDs. The cabinet-sized 360 had a performance comparable to a current low-end laptop computer.

- LEDs served to verify function of printed circuit boards (PCBs)
- LEDs served to show status of central processing unit (CPU)

History of GaP red and green LEDs

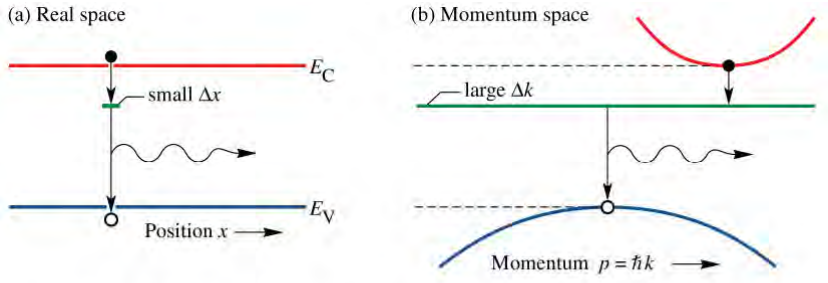

Fig. 1.5. (a) real-space and (b) momentum-space illustration of optical transitions in GaP doped with an optically active impurity level such as O or N, emitting in the red and green, respectively. GaP LEDs employ the *uncertainty principle* ($\Delta x\ \Delta p \geq \hbar$) which predicts that an electron wave function localized in real space is delocalized in momentum space thereby making possible momentum-conserving (vertical) transitions.

- There are direct-gap and indirect-gap semiconductors
- GaAs is direct but GaP is indirect
- Iso-electronic impurities (such as N and Zn-O) enable light emission

Red GaP LEDs

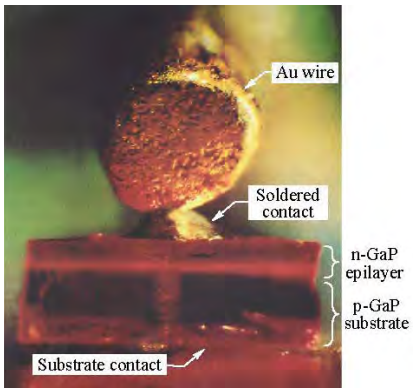

Fig. 1.6. GaP light-emitting diode grown by liquid-phase epitaxy emitting "brilliant red light" from the Zn- and O-doped p-n junction region (courtesy of Pilkuhn, 2000).

- N results in green emission
- Zn-O results in red emission
- However, efficiency is limited

Application for GaP:N green LEDs

Fig. 1.7. AT&T telephone set ("Trimline" model) with the dial pad illuminated by two green N-doped GaP LEDs. The illuminated dial pad was one of the first applications of green GaP:N LEDs.

- Dial pad illumination
- Telephone company (AT&T) decided that **green** is better color than **red**

LEDs in calculators

Fig. 1.8. Programmable pocket calculators Model SR-56 of the Texas Instruments Corporation and Model HP-67 of the Hewlett-Packard Corporation both manufactured starting in 1976. Seven-segment numeric characters composed of GaAsP LEDs were used in the display. The SR-56 came with a "huge" program memory of 100 steps. The HP-67 came with a magnetic card reader and had several freely programmable keys.

- LEDs were used in first generation of calculators
- Displayed numbers could not be seen in bright daylight
- LEDs consumed so much power that all calculators had rechargeable batteries

History of GaN blue, green, and white light emitters

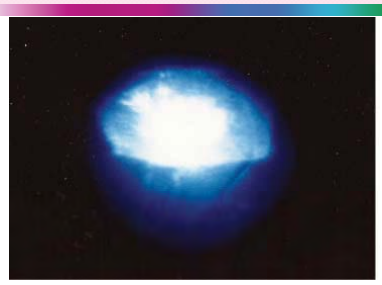

- Blue emission in GaN in 1972, Maruska et al., 1972
- However, no p-doping attained
- Devices were developed by RCA for three-color flat-panel display applications to replace cathode ray tubes (CRTs)

Fig. 1.11. Array of GaInN/GaN blue LEDs manufactured by the Nichia Corporation (after Nakamura and Fasol, 1997).

- Nichia Corporation (Japan) was instrumental in blue LED development
- Dr. Shuji Nakamura lead of development

Applications of green LEDs

Fig. 1.11. Green traffic signals are one of the ubiquitous applications of GaInN / GaN green LEDs.

Fig. 1.16. LED display consisting of 18 million LEDs located in New York City.

Fig. 1.17. Pedestrian sign indicating number of seconds left to cross street located in Taipei, Taiwan.

- High-brightness LEDs for outdoor applications

History of AlGaInP visible LEDs

Fig. 1.12. Example of red and amber AlGaInP / GaAs LEDs used in signage applications.

- Hewlett-Packard Corporation and Toshiba Corporation developed first high-brightness AlGaInP LEDs
- AlGaInP suited for red, orange, yellow, and yellow-green emitters

Recent applications ➔ High power applications

Fig. 1.13. (a) First goggle with integrated white LEDs used for (b) illumination during medical surgery (after Shimada *et al.*, 2001; Shimada *et al.*, 2003)

Fig. 1.14. Stone Bridge located in Regensburg, Germany, illuminated by LEDs.

Fig. 1.15. First automotive daytime running lights based on LEDs.

Radiative and nonradiative recombination

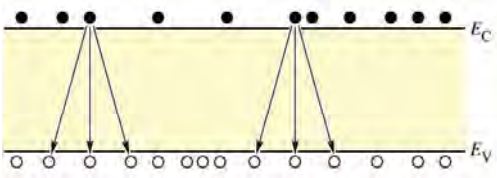

Fig. 2.1. Illustration of electron-hole recombination. The number of recombination events per unit time per unit volume is proportional to the product of electron and hole concentrations, *i. e.* $R \propto n\,p$.

- Recombination rate is proportional to the product of the concentrations of electrons and holes
- $R = B\,n\,p$

  where

  B = bimolecular recombination coefficient

  n = electron concentration

  p = hole concentration

Radiative electron-hole recombination

$$n = n_0 + \Delta n \qquad \text{and} \qquad p = p_0 + \Delta p$$

n	free electron concentration
n_0	equilibrium free electron concentration
Δn	excess electron concentration

$$R = -\frac{\mathrm{d}n}{\mathrm{d}t} = -\frac{\mathrm{d}p}{\mathrm{d}t} = B\,n\,p$$

R	recombination rate per cm^3 per s
B	bimolecular recombination coefficient

Carrier decay (low excitation)

$$\Delta n(t) = \Delta n_0\, \mathrm{e}^{-B(n_0+p_0)t}$$

$$\tau = \left[B\left(n_0 + p_0\right)\right]^{-1}$$

τ	carrier lifetime
B	bimolecular recombination coefficient

Radiative recombination for low-level excitation

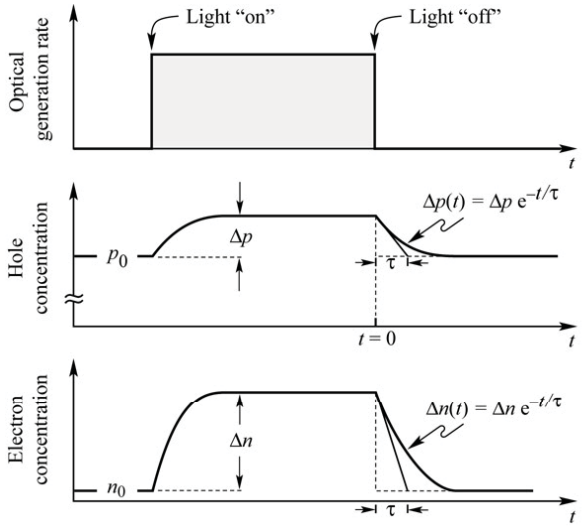

Fig. 2.2. Carrier concentration as a function of time before, during, and after an optical excitation pulse. The semiconductor is assumed to be p-type and thus $p_0 >> n_0$. Electrons and holes are generated in pairs, thus $\Delta p = \Delta n$. Under low-level excitation as shown here, it is $\Delta n << p_0$. In most practical cases the equilibrium minority carrier concentration is extremely small so that $n_0 << \Delta n$.

- Radiative lifetimes determine switch-on and switch-off times

Recombination lifetime: Theory versus experiment

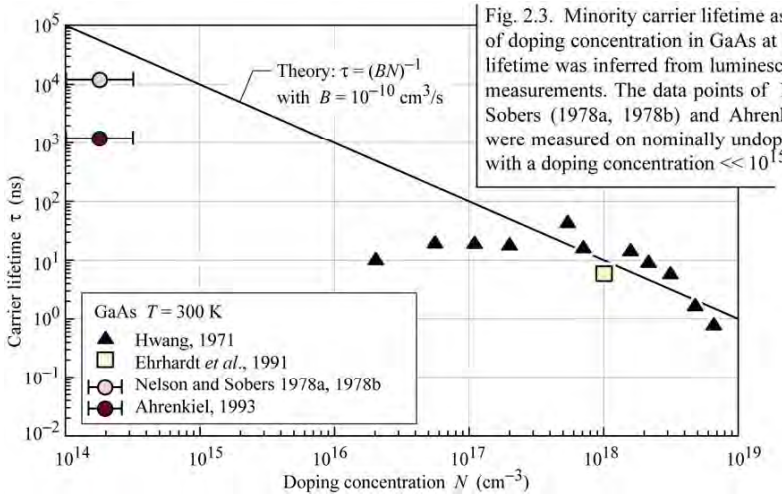

Fig. 2.3. Minority carrier lifetime as a function of doping concentration in GaAs at 300 K. The lifetime was inferred from luminescence decay measurements. The data points of Nelson and Sobers (1978a, 1978b) and Ahrenkiel (1993) were measured on nominally undoped material with a doping concentration $<< 10^{15}$ cm^{-3}.

- Radiative lifetime decreases with doping concentration

Nonradiative recombination in the bulk

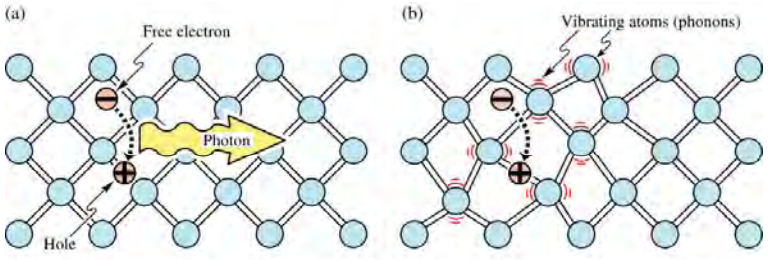

Fig. 2.5. (a) Radiative recombination of an electron-hole pair accompanied by the emission of a photon with energy $h\nu \approx E_g$. (b) In non-radiative recombination events, the energy released during the electron-hole recombination is converted to phonons (adopted from Shockley, 1950).

- Generation of heat competes with generation of light
- This is a very fundamental issue

Recombination mechanisms

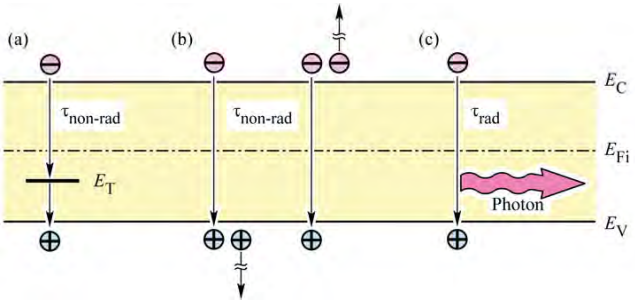

Fig. 2.6. Band diagram illustrating recombination: (a) non-radiative via deep level, (b) non-radiative via Auger process and (c) radiative.

- Recombination via deep levels
- Auger recombination
- Radiative recombination

Visualization of defects

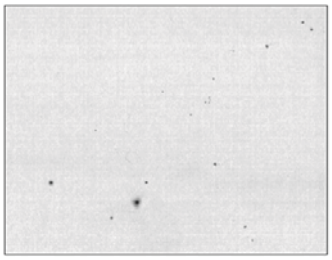

Fig. 2.7. Cathodoluminescence micrograph of a GaAs epitaxial layer. The dark spots are due to large clusters of non-radiative recombination centers (after Schubert, 1995).

- Dark spots are clusters of defects
- Dark spots are dark because lack of radiative recombination

Shockley-Read recombination

$$R_{SR} = \frac{p_0\,\Delta n + n_0\,\Delta p + \Delta n \Delta p}{\left(N_t v_p \sigma_p\right)^{-1}\left(n_0 + n_1 + \Delta n\right) + \left(N_t v_n \sigma_n\right)^{-1}\left(p_0 + p_1 + \Delta p\right)}$$

$$\frac{1}{\tau} = \frac{p_0 + n_0 + \Delta n}{\left(N_t v_p \sigma_p\right)^{-1}\left(n_0 + n_1 + \Delta n\right) + \left(N_t v_n \sigma_n\right)^{-1}\left(p_0 + p_1 + \Delta p\right)}$$

$$\tau_i = \tau_{n0}\left(1 + \frac{p_1 + n_1}{2n_i}\right) = \tau_{n0}\left[1 + \cosh\left(\frac{E_T - E_{Fi}}{kT}\right)\right]$$

- Mid-gap levels are effective non-radiative recombination centers

Nonradiative recombination at surfaces

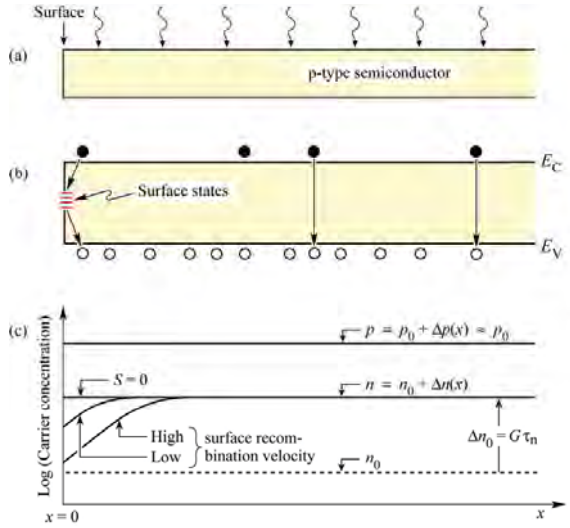

Fig. 2.9. (a) Illuminated p-type semiconductor, (b) band diagram, and (c) minority and majority carrier concentrations near the surface assuming uniform carrier generation due to illumination. The excess carrier concentrations are Δn and Δp.

- Surface recombination
- Surface recombination velocity

Surface recombination

$$n(x) = n_0 + \Delta n(x) = n_0 + \Delta n_\infty \left[1 - \frac{\tau_n S \exp(-x/L_n)}{L_n + \tau_n S} \right]$$

S	surface recombination velocity
x	distance from semiconductor surface
L_n	carrier diffusion length

Surface recombination velocities of semiconductors

GaAs	$S = 10^6$ cm/s
GaP	$S = 10^6$ cm/s
InP	$S = 10^3$ cm/s
GaN	$S = 10^3$ cm/s
Si	$S = 10^1$ cm/s

Demonstration of surface recombination

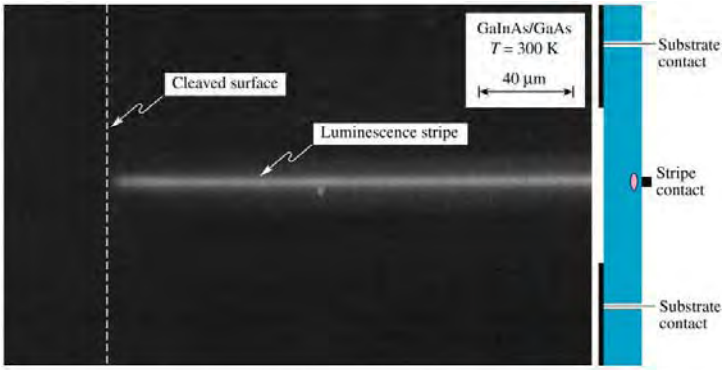

Fig. 2.10. Micrograph of a GaInAs/GaAs structure with a stripe-shaped contact on the top side and a contact widow at the substrate side of the device under current injection conditions. The luminescence emanating from the active region located below the stripe contact clearly decreases in the vicinity of the surface due to surface recombination.

- Making surface recombination "visible"

Competition: radiative & nonradiative recombination

$$\tau^{-1} = \tau_r^{-1} + \tau_{nr}^{-1}$$

$$\eta_{int} = \frac{\tau_r^{-1}}{\tau_r^{-1} + \tau_{nr}^{-1}}$$

τ	carrier lifetime
τ_{nr}	nonradiative carrier lifetime
τ_r	radiative carrier lifetime
η_{int}	internal quantum efficiency

LED basics: Electrical properties

Shockley equation for p-n junction diodes

$$I = e\,A\left(\sqrt{\frac{D_p}{\tau_p}}\,p_{n0} + \sqrt{\frac{D_n}{\tau_n}}\,n_{p0}\right)\left(e^{eV/kT} - 1\right)$$

$$= e\,A\left(\sqrt{\frac{D_p}{\tau_p}}\,\frac{n_i^2}{N_D} + \sqrt{\frac{D_n}{\tau_n}}\,\frac{n_i^2}{N_A}\right)\left(e^{eV/kT} - 1\right)$$

$$= I_s\left(e^{eV/kT} - 1\right)$$

where I_s is the saturation current

P-n junction band diagram

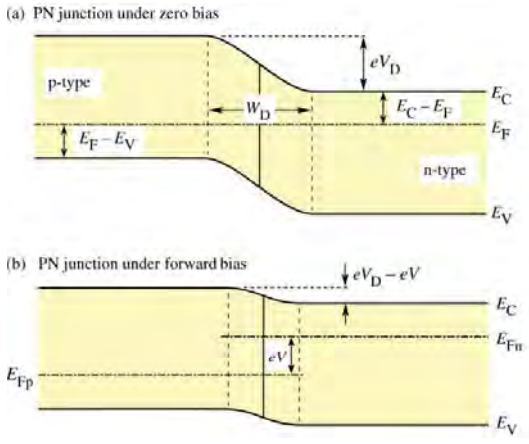

Fig. 4.1. P-N junction under (a) zero bias and (b) forward bias. Under forward bias conditions minority carriers diffuse into the neutral regions where they recombine.

Diode current-voltage characteristics

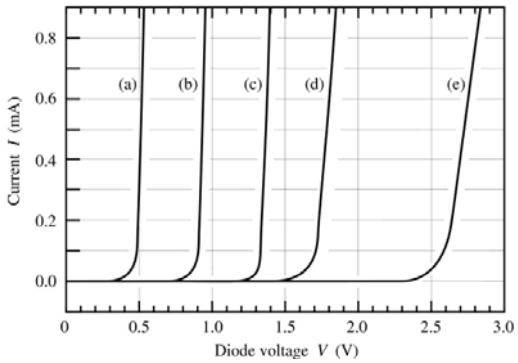

$T = 300$ K

(a)	Ge	$E_g \approx 0.7$ eV
(b)	Si	$E_g \approx 1.1$ eV
(c)	GaAs	$E_g \approx 1.4$ eV
(d)	GaAsP	$E_g \approx 2.0$ eV
(e)	GaInN	$E_g \approx 2.9$ eV

Fig. 4.2. Room temperature current - voltage characteristics of p-n junctions made of different semiconductors.

- Forward voltage is approximately equal to E_g / e

Diode forward voltage

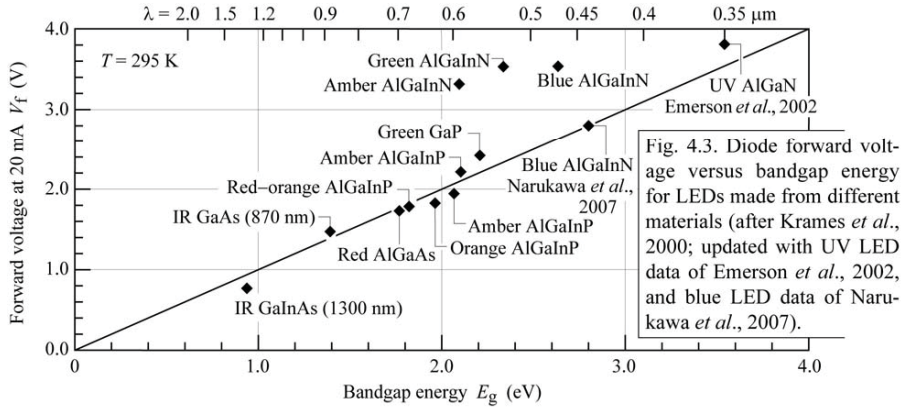

Fig. 4.3. Diode forward voltage versus bandgap energy for LEDs made from different materials (after Krames *et al.*, 2000; updated with UV LED data of Emerson *et al.*, 2002, and blue LED data of Narukawa *et al.*, 2007).

- UV-LEDs frequently show excess forward voltage

Deviations from ideal I-V characteristic

$$I = I_s \, e^{eV/(n_{ideal} kT)}$$

$$I - \frac{V - IR_s}{R_p} = I_s \, e^{e(V - IR_s)/(n_{ideal} kT)}$$

n_{ideal}	ideality factor
R_s	parasitic series resistance
R_p	parasitic parallel resistance

Non-ideal I-V characteristics

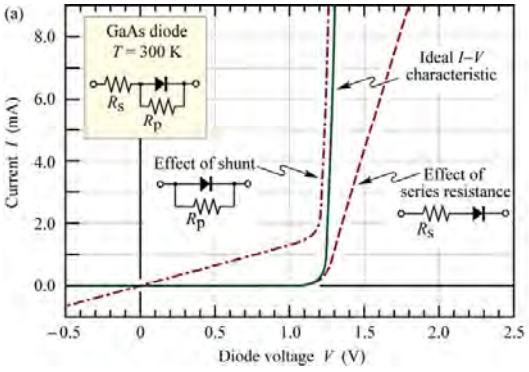

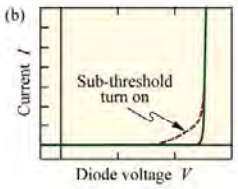

Fig. 4.4. (a) Effect of series and parallel resistance (shunt) on I–V characteristic. (b) I–V with clearly discernable sub-threshold turn-on, caused by defects or surface states.

- Problem areas of diode can be identified from I-V characteristic

Methods to determine series resistance

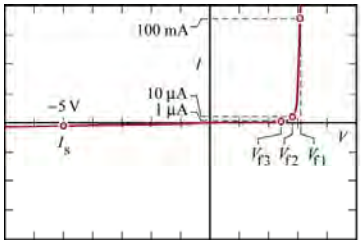

Fig. 4.6. Critical points of diode I–V characteristic, namely "forward voltage one", V_{f1} (measured at operating current, e.g. 100 mA), "forward voltage two", V_{f2} (measured at low current, e.g. 10 µA), "forward voltage three", V_{f3} (measured at very low current, e.g. 1 µA), and reverse saturation current (measured at e.g. – 5.0 V).

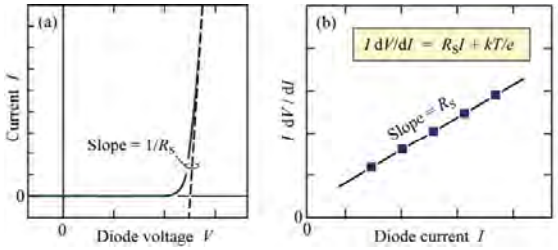

Fig. 4.7. Methods for evaluating diode series resistance. (a) Tangent for $V > V_{th}$ provides R_S. (b) Equation shown as inset is valid for forward bias ($V >> kT/e$).

- Method shown above suitable for series resistance measurement
- At high currents, diode I-V becomes linear due to dominance of series resistance. Diode series resistance can be extracted in linear regime

Carrier distribution in pn homo- and heterojunctions

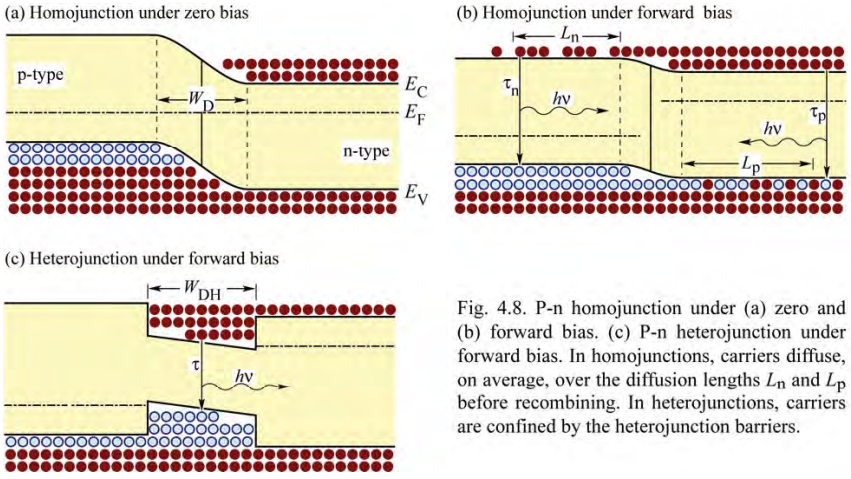

Fig. 4.8. P-n homojunction under (a) zero and (b) forward bias. (c) P-n heterojunction under forward bias. In homojunctions, carriers diffuse, on average, over the diffusion lengths L_n and L_p before recombining. In heterojunctions, carriers are confined by the heterojunction barriers.

- Double heterostructure enables high carrier concentrations in active region
  - A high efficiency results

Carrier overflow in double heterostructures

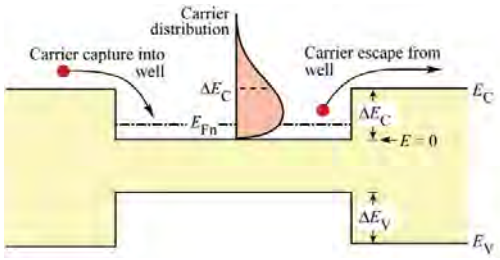

Fig. 4.11. Carrier capture and escape in a double heterostructure. Also shown is the carrier distribution in the active layer.

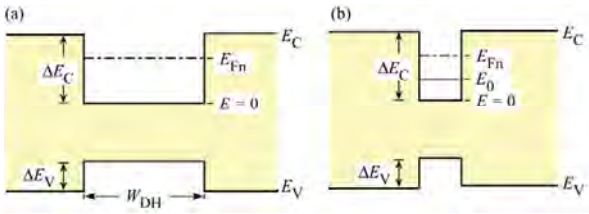

Fig. 4.12. Fermi level (E_{Fn}) and subband level (E_0) in (a) a double heterostructure and (b) a quantum well structure.

- Carrier leakage out of active region

Saturation of output power due to leakage

- A larger number of QWs reduce leakage

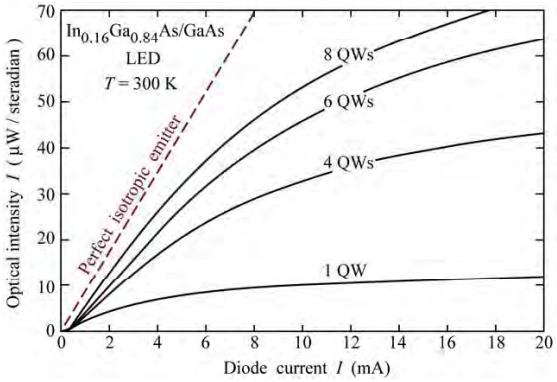

Fig. 4.13. Optical intensity emitted by $In_{0.16}Ga_{0.84}As/GaAs$ LEDs with active regions consisting of one, four, six, and eight quantum wells and theoretical intensity of a perfect isotropic emitter (dashed line) (after Hunt *et al.*, 1992).

Electron blocking layers

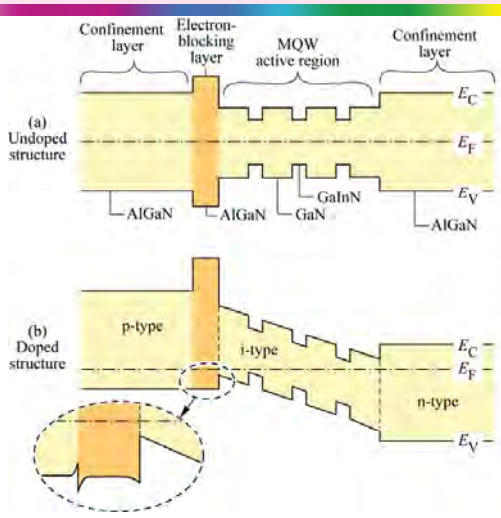

Fig. 4.14. AlGaN electron-blocking layer in an AlGaN/GaN/GaInN multi-quantum well structure. (a) Band diagram without doping. (b) Band diagram with doping. The Al content in the electron-blocking layer is higher than in the p-type confinement layer.

- Electron blocking layer
- Hole blocking layer
- Which of the two would be more effective?

Diode forward voltage

$$V = h\nu/e \approx E_g/e$$

$$V = \frac{E_g}{e} + IR_s + \frac{\Delta E_C - E_0}{e} + \frac{\Delta E_V - E_0}{e}$$

$I R_s$	resistive loss
$\Delta E_C - E_0$	electron energy loss upon injection into quantum well
$\Delta E_V - E_0$	hole energy loss upon injection into quantum well

LED basics: Optical properties

Internal, extraction, external, and power efficiency

$$\eta_{int} = \frac{\text{number of photons emitted from active region per second}}{\text{number of electrons injected into LED per second}} = \frac{P_{int}/(h\nu)}{I/e}$$

$$\eta_{extraction} = \frac{\text{number of photons emitted into free space per second}}{\text{number of photons emitted from active region per second}}$$

$$\eta_{ext} = \frac{\text{number of photons emitted into free space per sec.}}{\text{number of electrons injected into LED per sec.}} = \frac{P/(h\nu)}{I/e} = \eta_{int}\,\eta_{extraction}$$

$$\eta_{power} = \frac{P}{IV}$$ Power efficiency = Wall-plug efficiency = "Power out" / "power in"

Emission spectrum

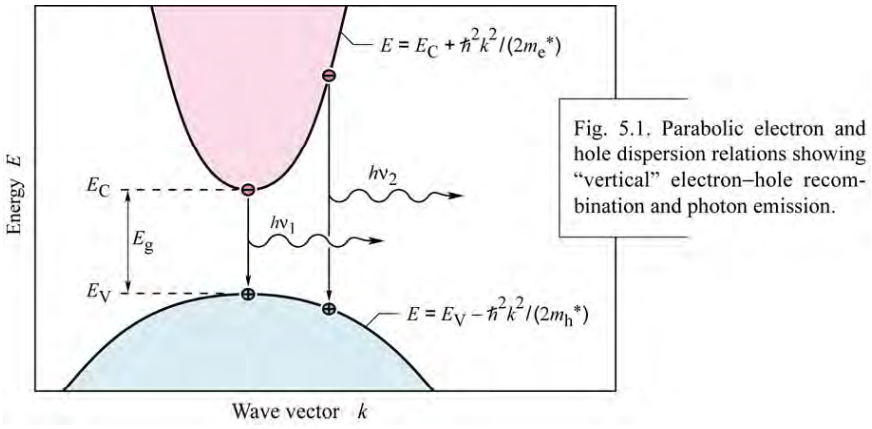

Fig. 5.1. Parabolic electron and hole dispersion relations showing "vertical" electron–hole recombination and photon emission.

- Electron and hole momentum must be conserved
- Photon has negligible momentum

Emission spectrum

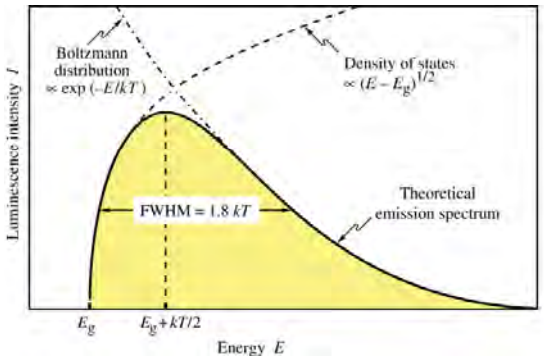

Fig. 5.2. Theoretical emission spectrum of an LED. The full width at half maximum (FWHM) of the emission line is 1.8 kT.

$$I(E) \propto \sqrt{E - E_g}\, e^{-E/(kT)}$$ $I(E)$ = emission spectrum

$$E = E_g + \frac{1}{2}kT$$ Energy of maximum emission intensity

$$\Delta E = 1.8\,kT$$ Spectral width

The light escape cone

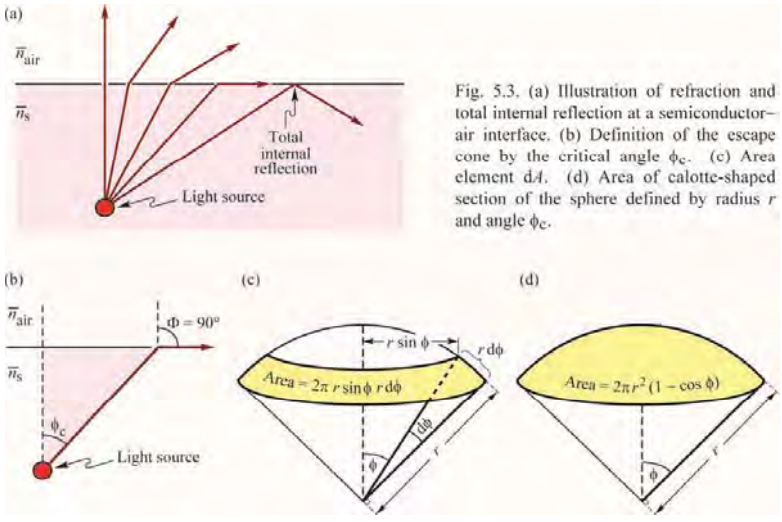

Fig. 5.3. (a) Illustration of refraction and total internal reflection at a semiconductor–air interface. (b) Definition of the escape cone by the critical angle ϕ_c. (c) Area element dA. (d) Area of calotte-shaped section of the sphere defined by radius r and angle ϕ_c.

- Total internal reflection occurs inside LED chip
- Light escape cone defined my critical angle for total internal reflection

Light escape in planar LEDs

- Above equation gives < 10 % extraction efficiency for typical III-V semiconductors

$$\frac{P_{\text{escape}}}{P_{\text{source}}} \approx \frac{1}{2}\left[1-\left(1-\frac{\phi_c{}^2}{2}\right)\right] = \frac{1}{4}\,\phi_c{}^2$$

- ϕ_c = critical angle of total internal reflection
- Problem: Only small fraction of light can escape from semiconductor

$$\frac{P_{\text{escape}}}{P_{\text{source}}} = \frac{1}{4}\,\frac{\bar{n}_{\text{air}}{}^2}{\bar{n}_s{}^2}$$

The lambertian emission pattern

$$I_{\text{air}} = \frac{P_{\text{source}}}{4\pi r^2}\,\frac{\bar{n}_{\text{air}}{}^2}{\bar{n}_s{}^2}\cos\Phi$$

I_{air}	emission intensity in air
Φ	angle with respect to surface normal

- Lambertian emission pattern has cosine-function dependence
- Diffuse sources also have lambertian emission pattern

Far-field patterns

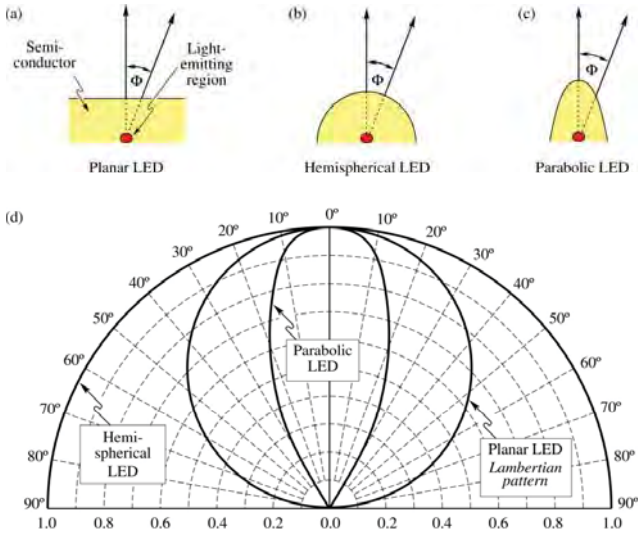

Fig. 5.5. Light-emitting diodes with (a) planar, (b) hemispherical, and (c) parabolic surfaces. (d) Far-field patterns of the different types of LEDs. At an angle of $\Phi = 60°$, the Lambertian emission pattern decreases to 50 % of its maximum value occuring at $\Phi = 0°$. The three emission patterns are normalized to unity intensity at $\Phi = 0°$.

- Die shaping can change emission pattern
- "Natural" LED has a planar surface

Effect of encapsulant

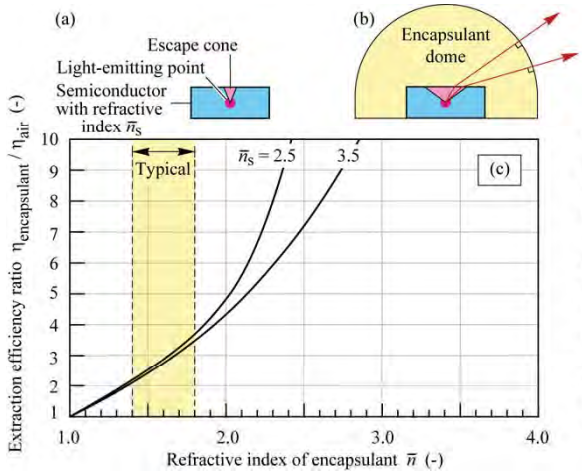

Fig. 5.6. LED (a) without and (b) with dome-shaped encapsulant. A larger escape angle is obtained for the LED with encapsulant dome. (c) Calculated ratio of light extraction efficiency emitted through the top surface of a planar LED with and without encapsulant dome. The refractive indices of typical epoxies range between 1.4 and 1.8 (adapted from Nuese *et al.*, 1969).

- Encapsulation material (such as epoxy or silicone) increases the light-extraction efficiency

Temperature dependence of emission intensity

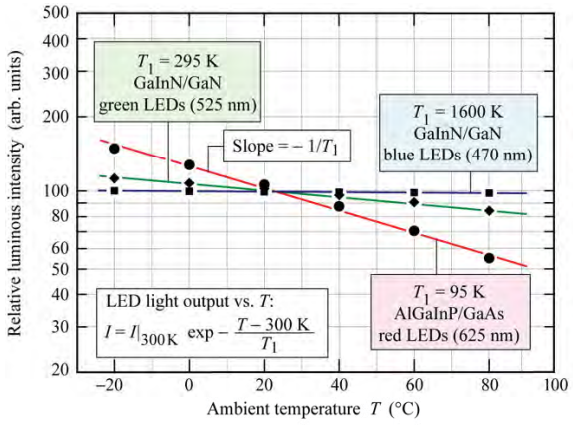

Fig. 5.7. Characteristic temperature T_1 of GaInN/GaN blue, GaInN/GaN green, and AlGaInP/GaAs red LEDs near room temperature (after data from Toyoda Gosei Corp., 2000). More recent data (Toyoda Gosei Corp., 2004) show the following values for T_1: Blue GaInN LED, 460 nm, T_1 = 1600 K; Cyan GaInN LED, 505 nm, T_1 = 832 K; Green GaInN LED, 525 nm, T_1 = 341 K; Red AlGaInP LED, 625 nm, T_1 = 199 K.

- Temperature dependence is characterized in terms of a characteristic temperature T_1
- $I = I_0 \exp(-T / T_1)$
- High T_1 is desirable

Temperature dependence of diode voltage

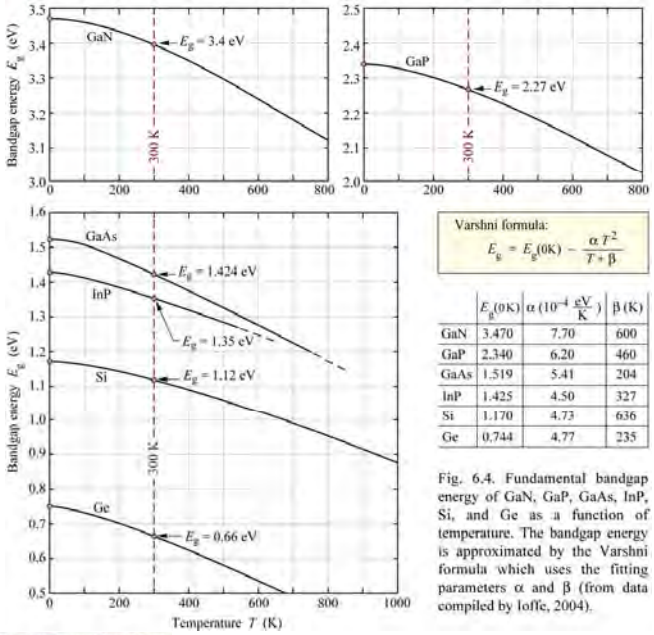

Varshni formula:

$$E_g = E_g(0K) - \frac{\alpha T^2}{T + \beta}$$

	E_g(0K)	α (10^{-4} eV/K)	β (K)
GaN	3.470	7.70	600
GaP	2.340	6.20	460
GaAs	1.519	5.41	204
InP	1.425	4.50	327
Si	1.170	4.73	636
Ge	0.744	4.77	235

Fig. 6.4. Fundamental bandgap energy of GaN, GaP, GaAs, InP, Si, and Ge as a function of temperature. The bandgap energy is approximated by the Varshni formula which uses the fitting parameters α and β (from data compiled by Ioffe, 2004).

- Diode voltage decreases with increasing temperature due to decrease in energy gap and increase in saturation current density

Temperature dependence of diode voltage

- Diode forward voltage can be used to assess junction temperature with high accuracy

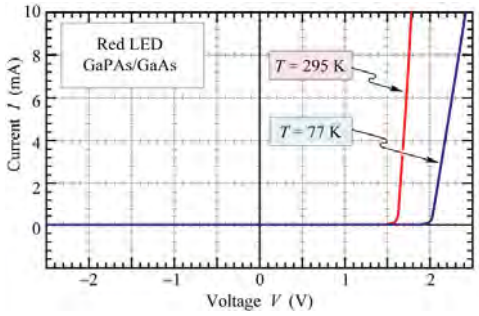

Fig. 6.5. Current–voltage characteristic of GaAsP/GaAs LED emitting in the red part of the visible spectrum, measured at 77 and 295 K. The threshold voltages are 2.0 and 1.6 V, at 77 and 300 K, respectively.

Drive circuits

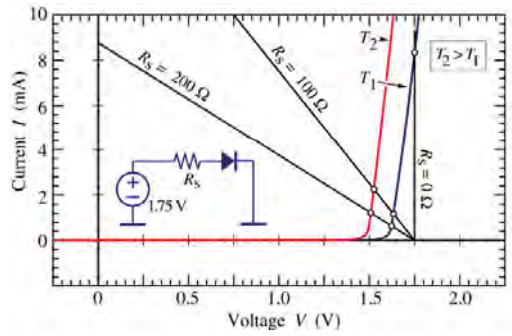

Fig. 4.16. LED drive circuit with series resistance R_S. The intersection between the diode *I-V*s and the load lines are the points of operation. Small series resistances result in an increased diode current at high temperatures, thus allowing for compensation of a lower LED radiative efficiency.

Constant-current drive circuit

Constant-voltage drive circuit

What are the advantages and disadvantages?

High internal efficiency LED designs

Double heterostructures

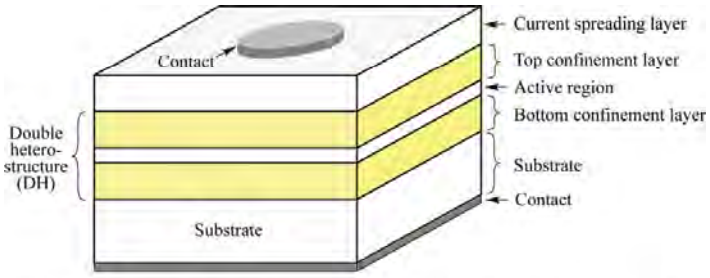

Fig. 7.1. Illustration of a double heterostructure consisting of a bulk or quantum well active region and two confinement layers. The *confinement* layers are frequently called *cladding* layers.

- Confinement of carriers in active region of double heterostructure (DH)
- High carrier concentration in active region

Homostructures versus double heterostructures

- High carrier concentration in active region of DH

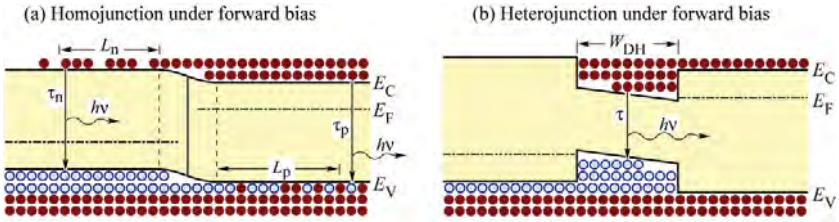

Fig. 7.2. Free carrier distribution in (a) a homojunction and (b) a heterojunction under forward bias conditions. In homojunctions, carriers are distributed over the diffusion length. In heterojunctions, carriers are confined to the well region.

Efficiency versus active layer thickness

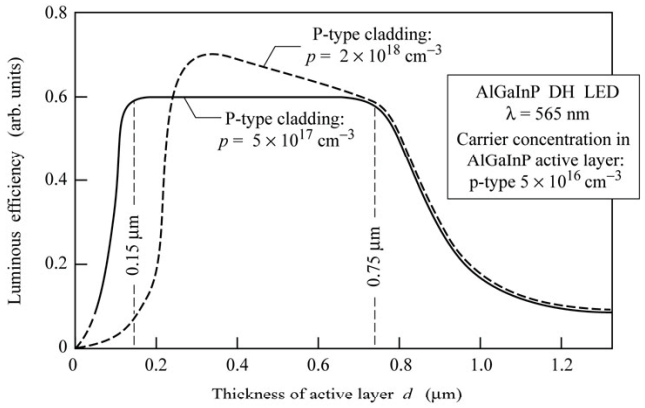

Fig. 7.3. Dependence of the luminous efficiency of an AlGaInP double heterostructure LED emitting at 565 nm on the active layer thickness. The figure reveals an optimum active region thickness of 0.15−0.75 µm (after Sugawara *et al*., 1992).

- Why is there a lower and upper limit for high efficiency?

Doping of active region

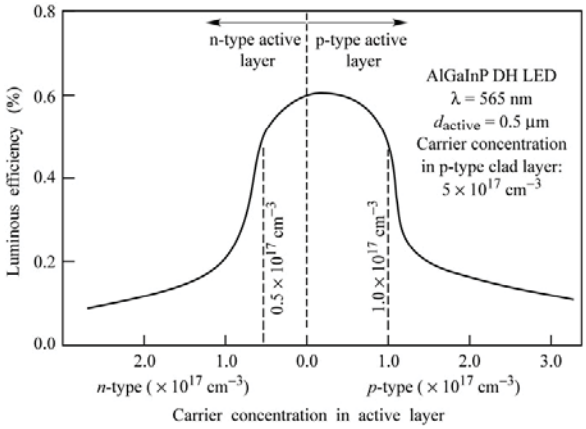

Fig. 7.4. Dependence of the luminous efficiency of an AlGaInP double heterostructure LED emitting at 565 nm on the active layer doping concentration (after Sugawara *et al*., 1992).

- Why is undoped active region optimum?

Non-radiative recombination and lifetime

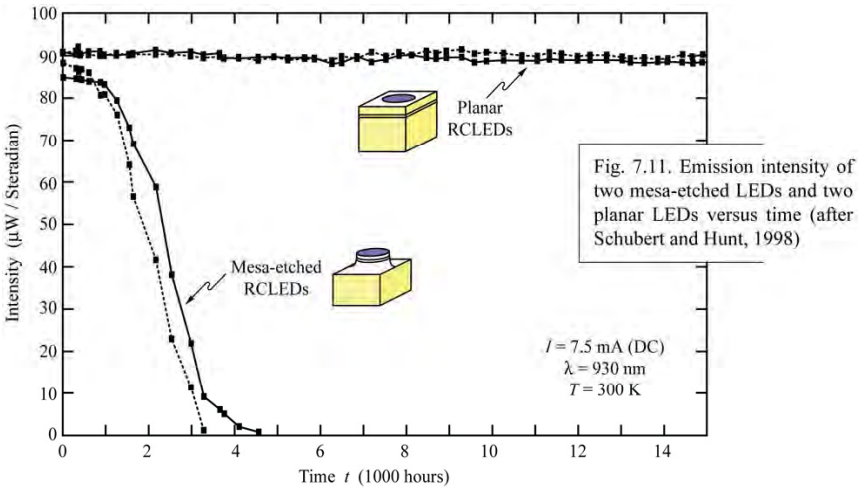

Fig. 7.11. Emission intensity of two mesa-etched LEDs and two planar LEDs versus time (after Schubert and Hunt, 1998)

- Device reliability affected by surface recombination

Lattice matching

- Lattice matching crucial for high efficiency
- Multitude of defects are created in mismatched material systems

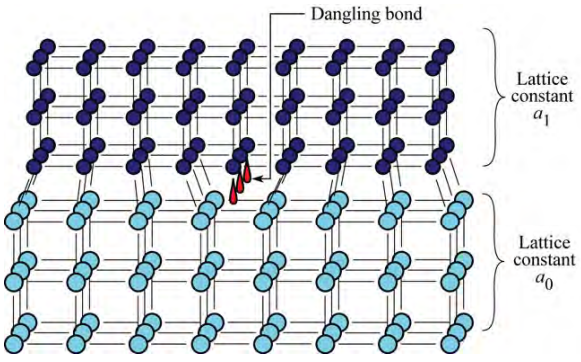

Fig. 7.12. Illustration of two crystals with mismatched lattice constant resulting in dislocations at or near the interface between the two semiconductors.

Lattice matching

- Dark lines due to dislocation lines
- Radiative efficiency low at dislocation lines

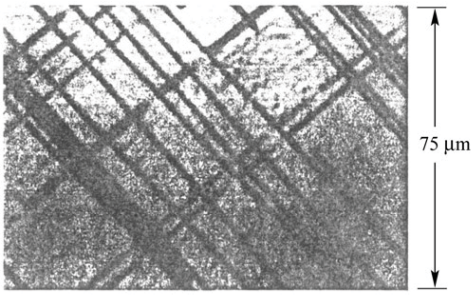

Fig. 7.13. Cathodo-luminescence image of a 0.35 µm thick $Ga_{0.95}In_{0.05}As$ layer grown on a GaAs substrate. The dark lines forming a cross-hatch pattern are due to misfit dislocations (after Fitzgerald *et al.*, 1989).

Pseudomorphic layers

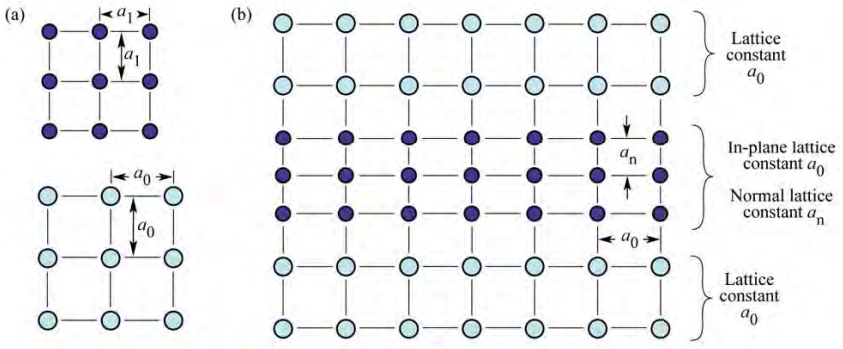

Fig. 7.14. (a) Cubic-symmetry crystals with equilibrium lattice constant a_1 and a_0. (b) Thin, coherently strained layer with equilibrium lattice constant a_1 sandwiched between two semiconductors with equilibrium lattice constant a_0. The coherently strained layer assumes an in-plane lattice constant a_0 and a normal lattice constant a_n.

- Thin layers can be elastically strained without incurring defects

Lattice matching

- Lattice matching better than 0.2 % required in AlGaInP material system
- Major challenge: High-quality crystal growth on mismatched substrates

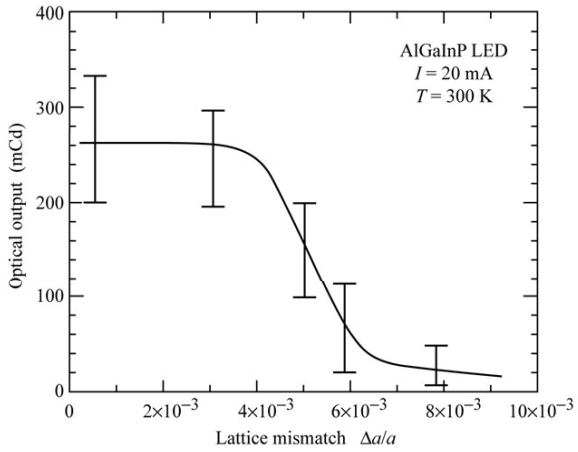

Fig. 7.15. Optical output intensity of an AlGaInP LED driven with an injection current of 20 mA versus the lattice mismatch between the AlInGaP active region and the GaAs substrate (after Watanabe and Usui, 1987).

Design of current flow

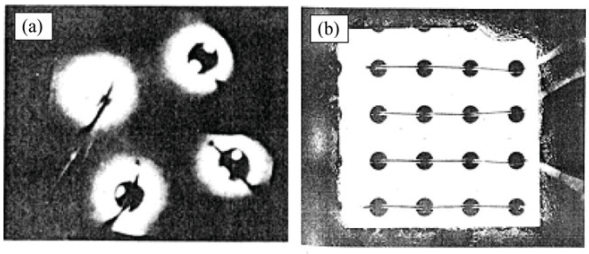

Fig. 8.1. Effect of the current-spreading layer on LED output. (a) Top view without a current-spreading layer. Emission occurs only near the perimeter of the contact. (b) Top view with a current-spreading layer (after Nuese *et al*., 1969).

- Light is generated under top contact
- Top contact shadows light
- Current spreading layer spreads current to edges of the LED die

Current-spreading layer

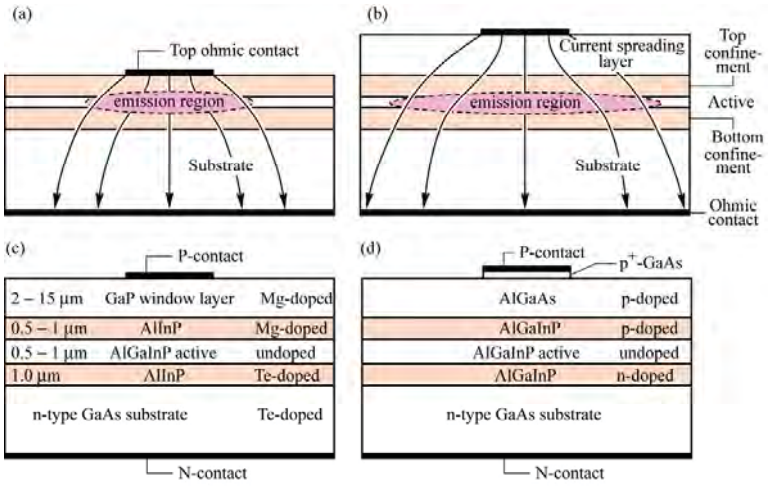

Fig. 8.2. Current-spreading structures in high-brightness AlGaInP LEDs. Illustration of the effect of a current-spreading layer for LEDs (a) without and (b) with a spreading layer on the light extraction efficiency. (c) GaP current-spreading structure (Fletcher *et al.*, 1991a, 1991b). (d) AlGaAs currect-spreading structure (Sugawara *et al.*, 1992a, 1992b).

Current-spreading layer

- Depression in center is due to top contact

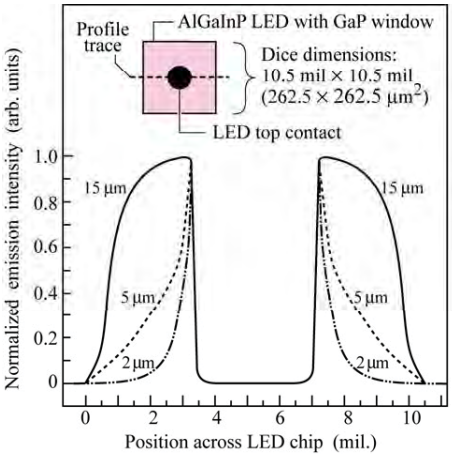

Fig. 8.3. The effect of GaP window thickness on current spreading is illustrated by surface light emission intensity profiles for three different AlGaInP LED chips with window layer thicknesses of 2, 5, and 15 µm. The profile is indicated by the dashed line in the inset. The dip in the middle of the profiles is due to the opaque ohmic contact pad. A microscope fitted with a video camara was used in the measurements (after Fletcher *et al.*, 1991a).

- **Current spreading layer** also called **window layer**

Current-spreading layer

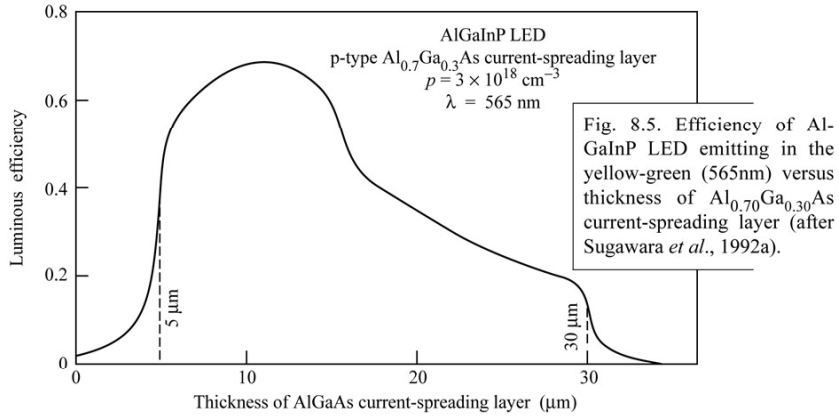

Fig. 8.5. Efficiency of AlGaInP LED emitting in the yellow-green (565nm) versus thickness of $Al_{0.70}Ga_{0.30}As$ current-spreading layer (after Sugawara *et al*., 1992a).

- Why is there a lower limit and an upper limit for the optimum thickness of the current-spreading layer?

Theory of current spreading

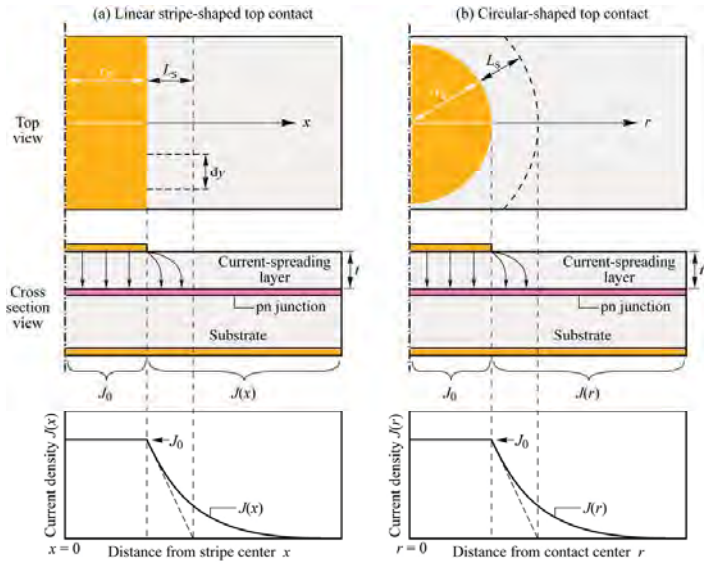

Fig. 8.6. Schematic illustration of current spreading in structures with different top contact geometries. (a) Linear stripe contact geometry. (b) Circular contact geometry.

Theory of current spreading

Current spreading length

$$L_s = \sqrt{\frac{t\, n_{ideal}\, kT}{\rho\, J_0\, e}}$$

$$t = \rho\, L_s^2\, J_0 \frac{e}{n_{ideal}\, kT}$$

t = thickness of current spreading layer

Current crowding in LEDs on insulating substrates

- Current chooses “path of least resistance”
- How can current crowding be reduced?

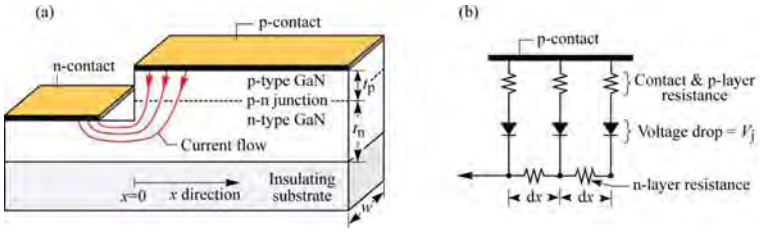

Fig. 8.8. (a) Current crowding in a mesa-structure GaN-based LED grown on an insulating substrate. (b) Equivalent circuit consisting of n-type and p-type layer resistances, p-type contact resistance, and ideal diodes representing the p-n junction.

Theory of current crowding

Theory of current crowding in LEDs on insulating substrates

$$J(x) = J(0)\exp\left(-x/L_s\right)$$

$$L_s = \sqrt{(\rho_c + \rho_p t_p)\, t_n / \rho_n}$$

L_s = current spreading length

Experimental evidence of current crowding

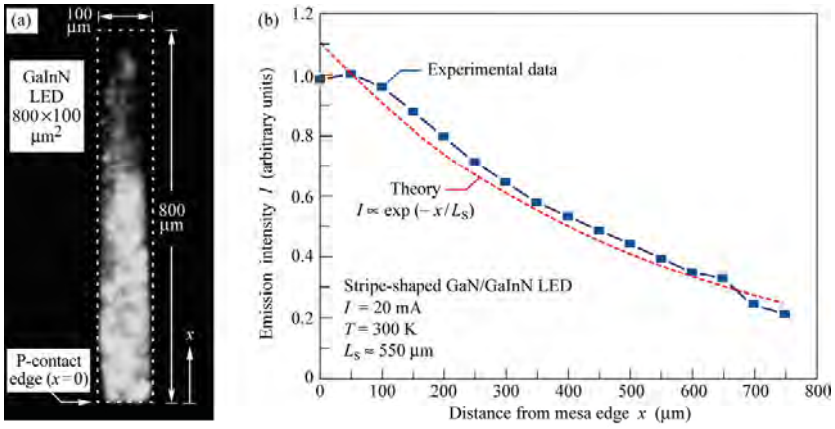

Fig. 8.9. (a) Micrograph of optical emission from mesa-structure GaInN/GaN LED grown on an insulating sapphire substrate. The LED has a stripe-shaped 800 µm × 100 µm p-type contact. (b) Theoretical and experimental emission intensity versus the distance from the mesa edge (after Guo and Schubert, 2001).

- Non-uniform light emission clearly observable

Current blocking layers

- Blocking layers require epitaxial regowth

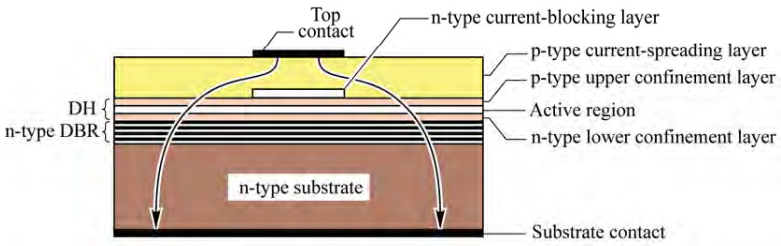

Fig. 8.13. LED with an n-type current-blocking layer located on the upper confinement layer. Light emission occurs in the regions not covered by the opaque top ohmic contact. The LED is fabricated by *epitaxial regrowth*. After growth of the current-blocking layer, the wafer is taken out of the growth system for etching. The wafer is then re-introduced into the epitaxial system for growth of the current-spreading layer.

High extraction efficiency structures

Absorption of below-bandgap light in semiconductors

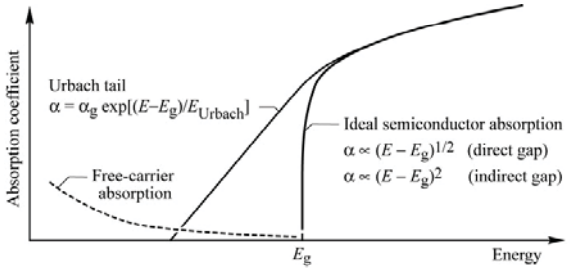

Fig. 9.1. Absorption coefficient of a semiconductor with bandgap E_g versus energy. The "Urbach tail" dominates absorption near but below the bandgap. Absorption further below the bandgap is dominated by free-carrier absorption.

- Free-carrier absorption (below bandgap)
- Urbach tail (below bandgap)

Double heterostructures

- Double heterostructures (DHs) are optically transparent
- All efficient LED designs use a DH

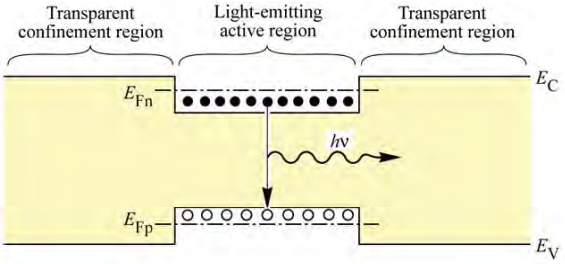

Fig. 9.2. Double hetero-structure with optically transparent confinement regions. Reabsorption in the active region is unlikely due to the high carrier concentration in the active region and the resulting Burstein–Moss shift of the absorption edge.

Shaping of LED dies

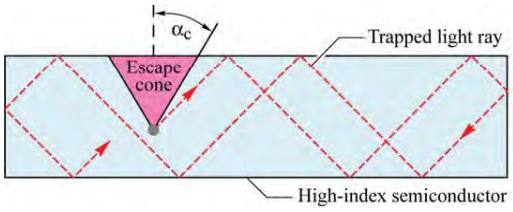

Fig. 9.3. "Trapped light" in a rectangular-parallelepiped-shaped semiconductor unable to escape for emission angles greater than α_c due to total internal reflection.

- Light "rattles around" and cannot escape
- Die shaping promises advantages
- Die shaping can be expensive

Shaping of LED dies

- Are these structure practical?

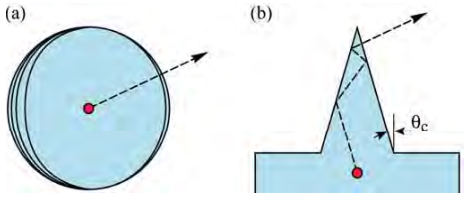

Fig. 9.4. Schematic illustration of different geometric shapes for LEDs with perfect extraction efficiency. (a) Spherical LED with a point-like light-emitting region at the center of the sphere. (b) A cone-shaped LED.

Rectangular parallelepiped shape versus cylinder

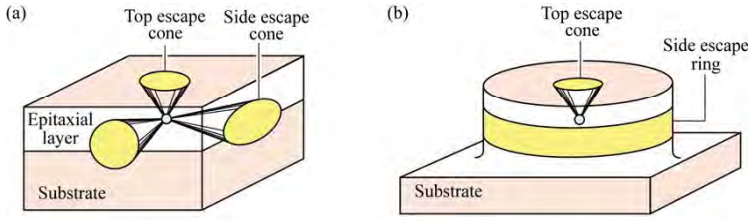

Fig. 9.5. Illustration of different geometric shapes of LEDs. (a) Rectangular parallelepipedal LED die with a total of six escape cones. (b) Cylindrical LED die with a top escape cone and a side escape ring.

- Cylinder shape advantageous over parallelepiped shape
- Additional cost of cylinder shape?

Truncated inverted pyramid (TIP) LED

- Additional cost of die shaping

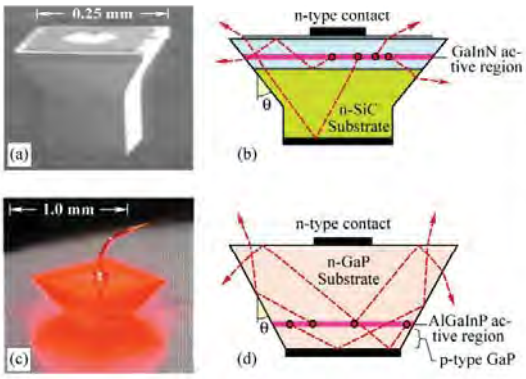

Fig. 9.6. Die-shaped devices: (a) Blue GaInN emitter on SiC substrate with trade name "Aton". (b) Schematic ray traces illustrating enhanced light extraction. (c) Micrograph of truncated inverted pyramid (TIP) AlGaInP/GaP LED. (d) Schematic diagram illustrating enhanced extraction (after Osram, 2001; Krames *et al.*, 1999).

Truncated inverted pyramid (TIP) LED

- One of the most efficient LED designs

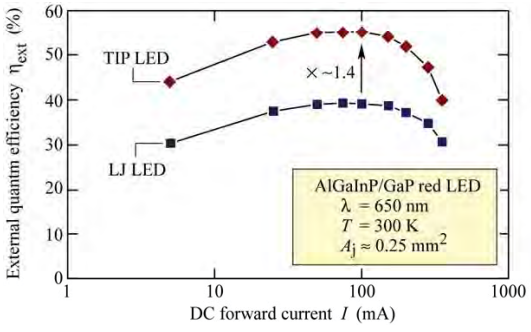

Fig. 9.7. External efficiency vs. forward current for red-emitting (650 nm) truncated inverted pyramid (TIP) LEDs and large junction (LJ) LEDs mounted in power-lamp packages. The TIP LED exhibits a 1.4 times improvement in extraction efficiency compared with the LJ device, resulting in a peak external quantum efficiency of 55 % at 100 mA (after Krames *et al.*, 1999).

Cross-shaped contacts and other contact geometries

- Circular top contact suited for small LEDs
- Large-die LEDs require different contact geometries

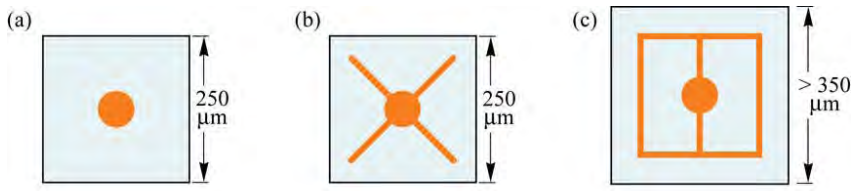

Fig. 9.11. Top view of an LED die with (a) a circular contact also serving as a bond pad and (b) a cross-shaped contact with a circular bond pad. (c) Typical contact geometry used for larger LED dies.

Transparent substrate technology

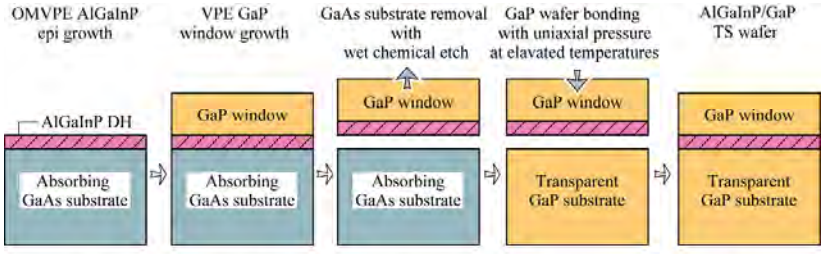

Fig. 9.12. Schematic fabrication process for wafer-bonded transparent substrate (TS) AlGaInP/GaP LEDs. After the selective removal of the original GaAs substrate, elevated temperature and uniaxial pressure are applied, resulting in the formation of a single TS LED wafer (after Kish *et al.*, 1994).

- Regular AlGaInP LEDs are grown on GaAs substrates
- GaAs is absorbing (absorbing substrate = AS)
  - ➔ Transparent-substrate (TS) technology

AS versus TS technology

- Transparent substrate (TS) clearly better than absorbing substrate (AS)

(a) AS LED

(b) TS LED

Fig. 9.14. (a) Amber AlGaInP LED with a GaP window layer and absorbing GaAs substrate (AS). (b) Amber AlGaInP LED with a GaP window layer and a transparent GaP substrate (TS) fabricated by wafer bonding. Conductive Ag-loaded die-attach epoxy can be seen at bottom (after Kish and Fletcher, 1997).

Anti-reflection optical coatings

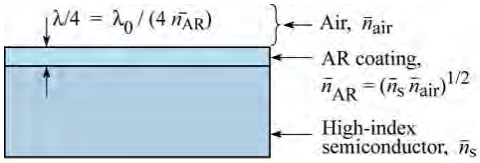

Fig. 9.15. Illustration of optimum thickness and refractive index of an anti-reflection (AR) coating.

$$R = \frac{(\bar{n}_s - \bar{n}_{air})^2}{(\bar{n}_s + \bar{n}_{air})^2}$$

Table: Refractive index and transparency range of common dielectrics suitable as anti-reflection (AR) coatings (after Palik, 1998)

Dielectric material	*Refractive index*	*Transparency range*
SiO_2 (Silica)	1.45	> 0.15 μm
Al_2O_3 (Alumina)	1.76	> 0.15 μm
TiO_2 (Titania)	2.50	> 0.35 μm
Si_3N_4	2.00	> 0.25 μm
ZnS	2.29	> 0.34 μm
CaF_2	1.43	> 0.12 μm

LED with Reflectors

- Metal reflectors and DBRs
- DBR = Distributed Bragg reflector
- DBRs reduce reflection losses

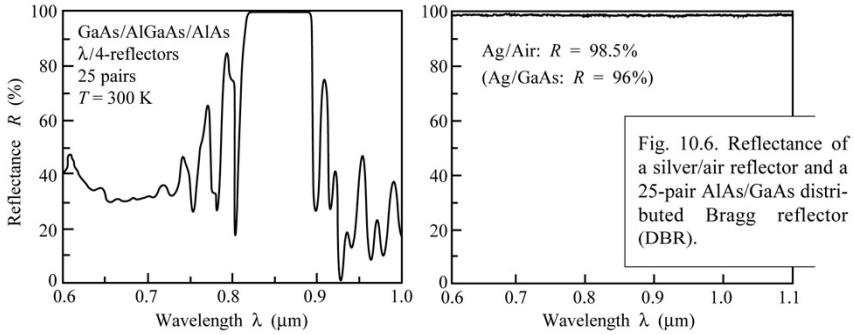

Fig. 10.6. Reflectance of a silver/air reflector and a 25-pair AlAs/GaAs distributed Bragg reflector (DBR).

LED with Reflectors

- DBR = Distributed Bragg reflector
- DBRs reduce reflection losses

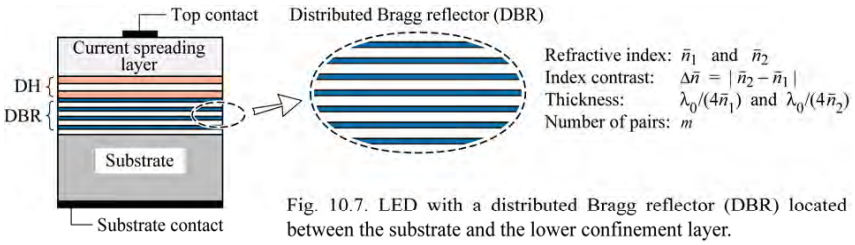

Fig. 10.7. LED with a distributed Bragg reflector (DBR) located between the substrate and the lower confinement layer.

Distributed Bragg reflectors

$$t_{l,h} = \lambda_{l,h} / 4 = \lambda_0 / (4\,\bar{n}_{l,h})$$

… valid for normal incidence

$$t_{l,h} = \lambda_{l,h} / (4\cos\Theta_{l,h}) = \lambda_0 / (4\,\bar{n}_{l,h}\cos\Theta_{l,h})$$

… valid for oblique incidence

DBRs

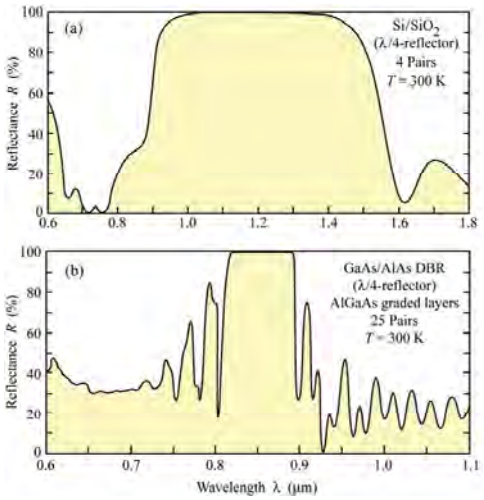

Fig. 10.8. Reflectance of two distributed Bragg reflectors (DBRs) versus wavelength. (a) Four-pair Si/SiO_2 reflector with high index contrast. (b) 25-pair AlAs/GaAs reflector. The high-index-contrast DBR only needs four pairs to attain high reflectivity. Note that the stop band of the high-index-contrast DBR is wider compared with the low-contrast DBR.

Parameters:

- Reflectivity
- Spectral width

DBRs

Material system	*Bragg wavelength*	n_{low}	n_{high}	Δn	*Transparency range*
$Al_{0.5}In_{0.5}P$ / GaAs	590 nm	3.13	3.90	0.87	> 870 nm (lossy)
$Al_{0.5}In_{0.5}P$ / $Ga_{0.5}In_{0.5}P$	590 nm	3.13	3.74	0.87	> 649 nm (lossy)
$Al_{0.5}In_{0.5}P$ / $(Al_{0.3}Ga_{0.7})_{0.5}In_{0.5}P$	615 nm	3.08	3.45	0.37	> 592 nm
$Al_{0.5}In_{0.5}P$ / $(Al_{0.4}Ga_{0.6})_{0.5}In_{0.5}P$	590 nm	3.13	3.47	0.34	> 576 nm
$Al_{0.5}In_{0.5}P$ / $(Al_{0.5}Ga_{0.5})_{0.5}In_{0.5}P$	570 nm	3.15	3.46	0.31	> 560 nm
AlAs / GaAs	900 nm	2.97	3.54	0.57	> 870 nm
SiO_2 / Si	1300 nm	1.46	3.51	2.05	> 1106 nm

Table 7.2. Properties of distributed Bragg reflector (DBR) materials used for visible and infrared LEDs. DBRs marked as 'lossy' are absorbing at Bragg wavelength (data after Adachi, 1990; Adachi *et al*., 1994; Kish and Fletcher, 1997; Babic *et al*., 1999; Palik, 1998).

Resonant-cavity light-emitting diodes

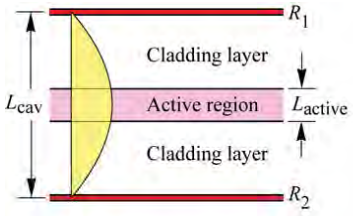

Fig. 15.1. Schematic illustration of a resonant cavity consisting of two metal mirrors with reflectivity R_1 and R_2. The active region has a thickness L_{active} and an absorption coefficient α. Also shown is the standing optical wave. The cavity length L_{cav} is equal to $\lambda/2$.

- Insert a light-emitting active region into an optical microcavity
- Optical mode density is changed
- Resonant cavity: Optical mode density has maximum at emission wavelength
- Enhanced spontaneous emission results

RCLED design rules

First design rule

$$R_1 \ll R_2$$

(Light-exit mirror should have lower reflectivity than back mirror)

Second design rule

Use shortest possible cavity length L_{cav}. Typically $L_{cav} = \lambda / 2$

Third design rule

$$2 \xi \alpha L_{active} < (1 - R_1)$$

(Absorption loss in active region should be smaller than the mirror loss of the light-exit mirror)

First RCLED

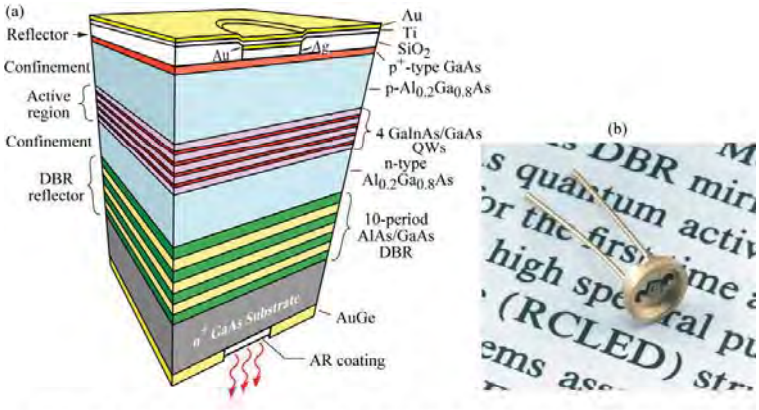

Fig. 15.4. (a) Schematic structure of a substrate-emitting GaInAs/GaAs RCLED consisting of a metal top reflector and a bottom distributed Bragg reflector (DBR). The RCLED emits at 930 nm. The reflectors are an AlAs/GaAs DBR and a Ag top reflector. (b) Picture of the first RCLED (after Schubert *et al.*, 1994).

- First RCLED had GaInAs active region and AlGaAs confinement layers

RCLED spectrum and performance

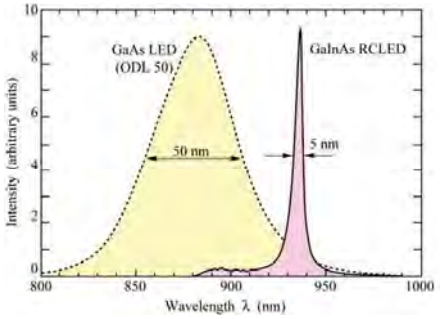

Fig. 15.6. Comparison of the emission spectra of a GaAs LED emitting at 870 nm (AT&T ODL 50 product) and a GaInAs RCLED emitting at 930 nm (after Hunt *et al.*, 1993).

- Narrow emission line

- High emission intensity along surface-normal direction

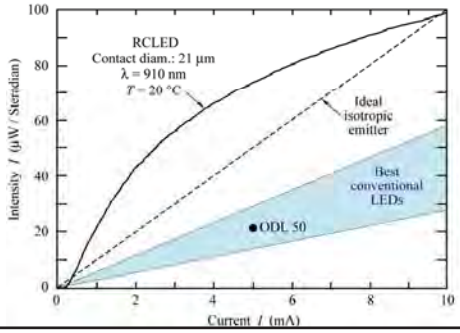

Fig. 15.7. Light-versus-current curves of a GaInAs/GaAs RCLED and of the *ideal isotropic emitter*. The ideal isotropic emitter is a hypothetial device emitting light isotropically with a quantum efficiency of 100%. The shaded region shows the intensity of the best conventional LEDs. The ODL 50 is a commercial LED product (after Schubert *et al.*, 1994).

650 nm RCLED for plastic optical fiber (POF) communications

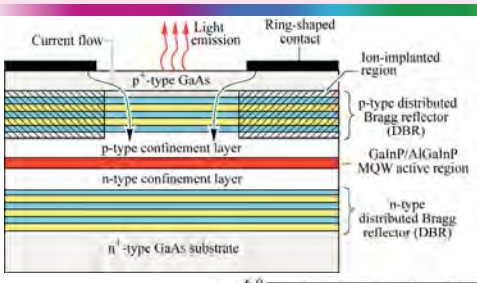

Fig. 15.9. Structure of a GaInP/AlGaInP/GaAs MQW RCLED emitting at 650 nm used for plastic optical fiber applications (after Whitaker, 1999)

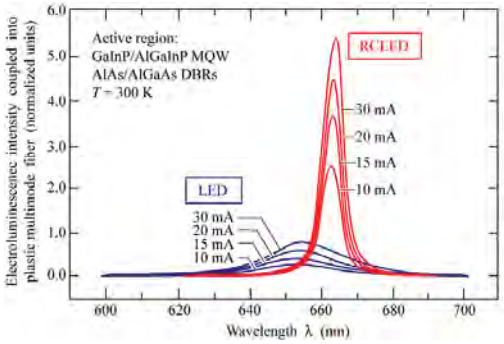

Fig. 15.12. Spectra of light coupled into a plastic optical fiber from a GaInP/AlGaInP MQW RCLED and a conventional GaInP/AlGaInP LED at different drive currents. Note the narrower spectrum and higher coupled power of the RCLED (after Streubel *et al.*, 1998).

- Plastic optical fibers (POFs) have loss minimum at about 550 – 650 nm

Packaging

Conventional packages provide

- Electrical path
- Optical path

Encapsulant dome

- Index contrast is reduced by epoxy dome ➔ increases light extraction
- Hermeticity, mechanical stability, chemical stability
- Encapsulants: Epoxy resin, PMMA, or silicone

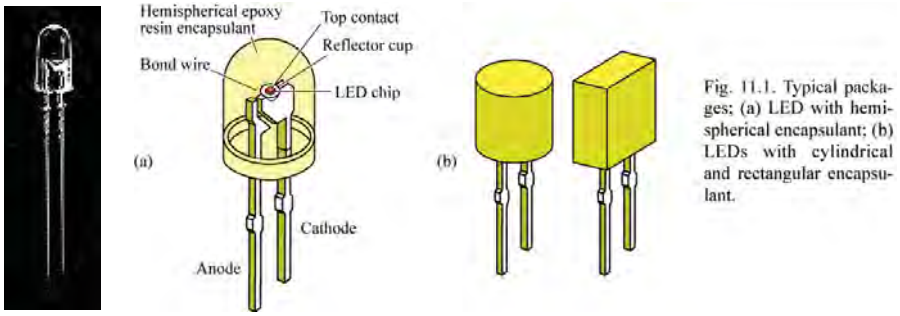

Fig. 11.1. Typical packages; (a) LED with hemispherical encapsulant; (b) LEDs with cylindrical and rectangular encapsulant.

Power package

Power packages provide

- Electrical path
- Optical path
- **Thermal path**

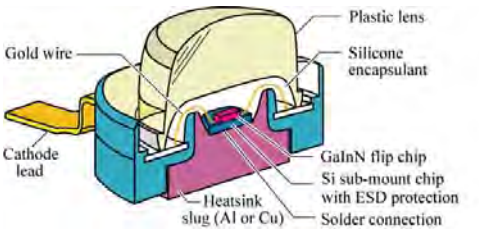

Fig. 11.2. Cross section through high-power package. The heatsink slug can be soldered to a printed circuit board for efficient heat removal. This package is called *Barracuda package* which was introduced by Lumileds Corp. (adopted from Krames, 2003).

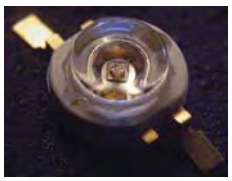

Flat glass versus lens package

- Examples of packages are shown below
  - Flat top package with an air cavity
    - These devices are injected with very high currents that also create much heat
  - Rounded top package
    - Silicone encapsulant
  - Side-emitting packages
    - For LCD display applications

Flat-top package | Rounded top package | Side-emitting package

Thermal resistance

- Rapid progress is being made with thermal resistance of packages
- **Figure of merit**: Thermal resistance = d*T*/d*P* where *T* = temperature increase and *P* = thermal power dissipated in package

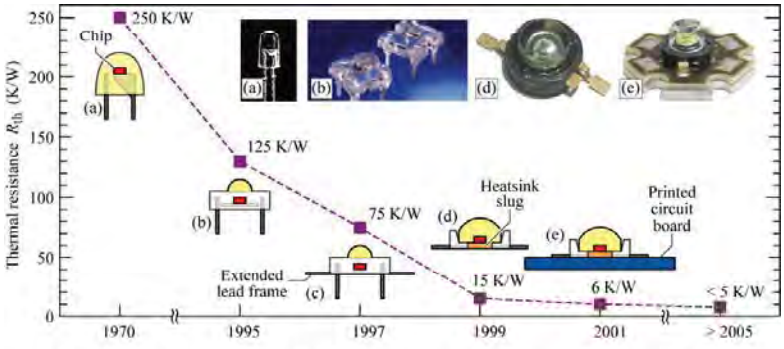

Fig. 11.5. Thermal resistance of LED packages: (a) 5mm (b) low-profile (c) low-profile with extended lead frame (d) heatsink slug (e) heatsink slug mounted on printed circuit board (PCB). Trade names for these packages are "Piranha" (b and c, Hewlett Packard Corp.), "Barracuda" (d and e, Lumileds Corp.), and "Dragon" (d and e, Osram Opto Semiconductors Corp.) (adopted from Arik *et al.*, 2002).

Visible-spectrum LEDs

The GaAsP, GaP, GaAsP:N and GaP:N material system

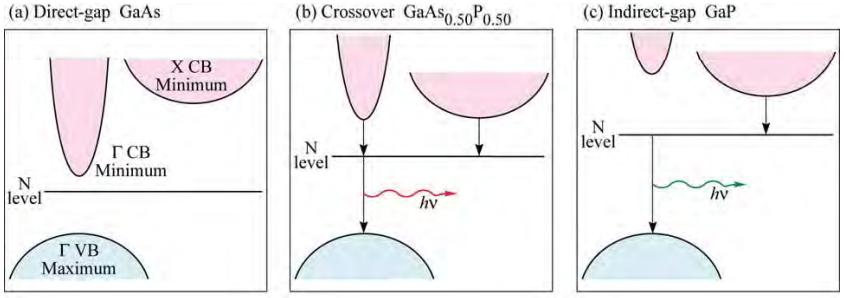

Fig. 12.1. Schematic band structure of GaAs, GaAsP, and GaP. Also shown is the nitrogen level. At a P mole fraction of 45–50%, the direct–indirect crossover occurs.

- Lattice mismatched system
- GaAsP suitable for indicator lights

GaAsP

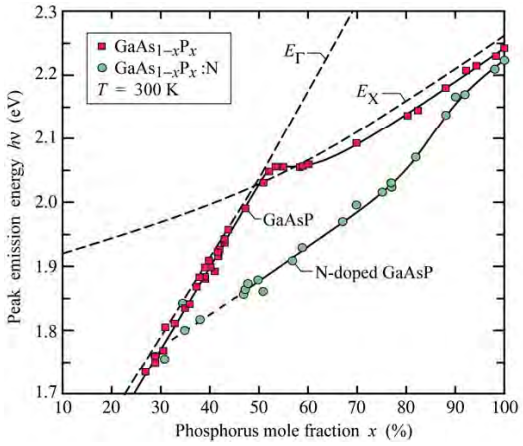

Fig. 12.2. Room-temperature peak emission energy versus alloy composition for undoped and nitrogen-doped GaAsP LEDs injected with a current density of 5 A/cm^2. Also shown is the energy gap of the direct-to-indirect ($E\Gamma$-to-E_X) transition. The direct–indirect crossover occurs at $x \approx 50\%$ (after Craford *et al.*, 1972).

- Material system has a direct-indirect transition

GaAsP

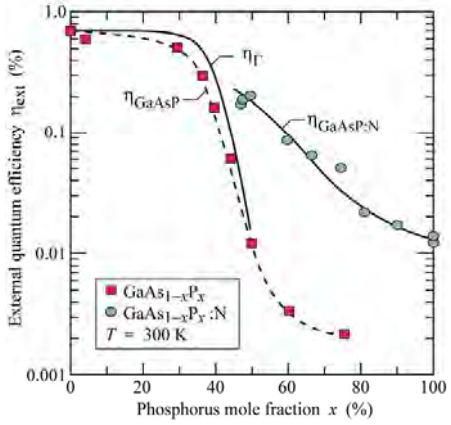

Fig. 12.3. Experimental external quantum efficiency of undoped and N-doped GaAsP versus the P mole fraction. Also shown is the calculated direct-gap (Γ) transition efficiency, η_Γ, and the calculated nitrogen (N) related transition efficiency, η_N (solid lines). Note that the nitrogen-related efficiency is higher than the direct-gap efficiency in the indirect bandgap (x > 50%) regime (after Campbell *et al.*, 1974).

Summary: The GaAsP, GaP, GaAsP:N and GaP:N material system has the fundamental problem of lattice mismatch and is not suitable for high-power LEDs

The AlGaAs/GaAs material system

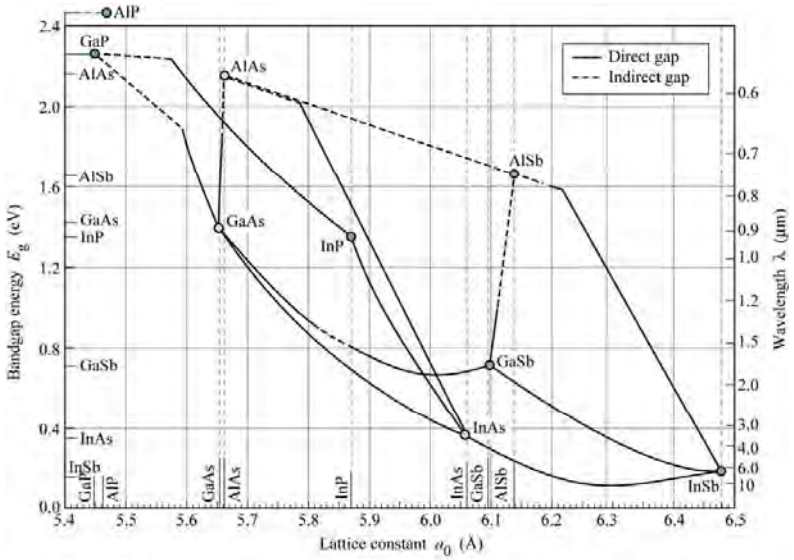

Fig. 12.6. Bandgap energy and lattice constant of various III–V semiconductors at room temperature (after Tien, 1988).

AlGaAs/GaAs

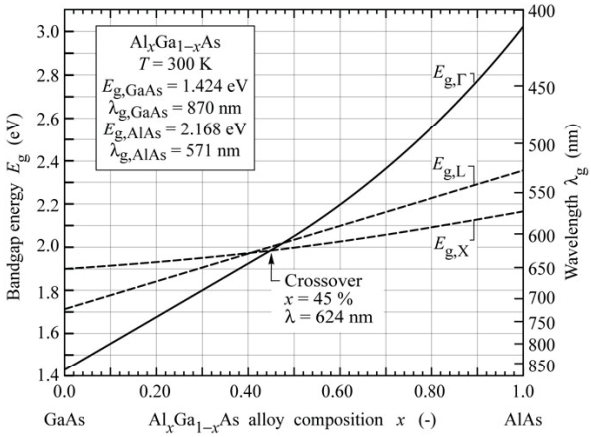

$E_{g,\Gamma}$ /eV = 1.424 + 1.247 x $(0 \le x \le 0.45)$
$E_{g,\Gamma}$ /eV = 1.424 + 1.247x + 1.147$(x - 0.45)$ $(0.45 \le x \le 1.0)$
$E_{g,L}$ /eV = 1.708 + 0.642 x $(0 \le x \le 1.0)$
$E_{g,X}$ /eV = 1.900 + 0.125 x + 0.143 x^2 $(0 \le x \le 1.0)$

Fig. 12.7. Bandgap energy and emission wavelength of AlGaAs at room temperature. E_Γ denotes the direct gap at the Γ point and E_L and E_X denote the indirect gap at the L and X point of the Brillouin zone, respectively (adapted from Casey and Panish, 1978).

- Material system has a direct-indirect transition

The AlGaInP/GaAs material system

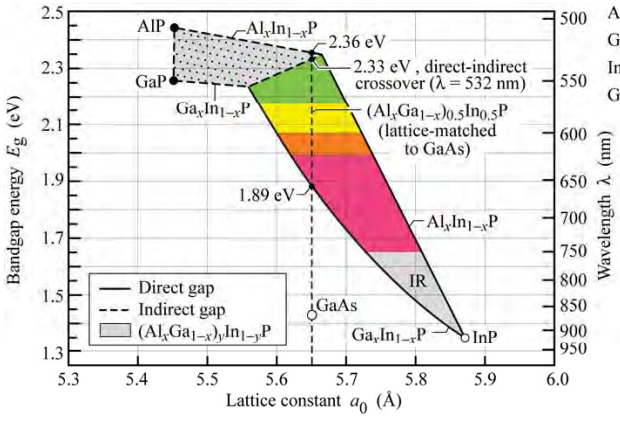

AlP: E_g = 2.45 eV, a_0 = 5.4510 Å
GaP: E_g = 2.26 eV, a_0 = 5.4512 Å
InP: E_g = 1.35 eV, a_0 = 5.8686 Å
GaAs: E_g = 1.424 eV, a_0 = 5.6533 Å

Fig. 12.9. Bandgap energy and corresponding wavelength versus lattice constant of $(Al_xGa_{1-x})_yIn_{1-y}P$ at 300 K. The vertical dashed line shows $(Al_xGa_{1-x})_{0.5}In_{0.5}P$ lattice matched to GaAs (adapted from Chen *et al.*, 1997).

- High-brightness system for red, orange, and yellow LEDs

AlGaInP/GaAs

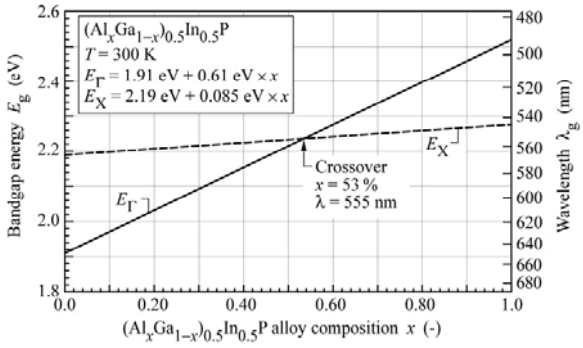

Fig. 12.10. Bandgap energy and emission wavelength of unordered AlGaInP lattice matched to GaAs at room temperature. E_Γ denotes the direct gap at the Γ point and E_X denotes the indirect gap at the X point of the Brillouin zone (after Prins *et al.*, 1995 and Kish and Fletcher, 1997).

- Material system has a direct-indirect transition

GaN material system

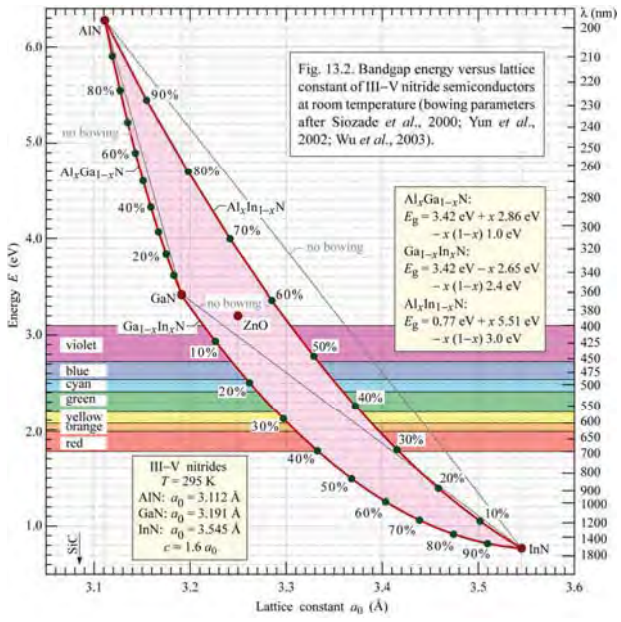

- ***Summary***: The GaInN material system is suited for UV, violet, blue, cyan and green high-power LEDs. Efficiency decreases in the green spectral range.

Optical characteristics of high-brightness LEDs

- Note that green emitter shows broadest emission line
- Green emitters need further development

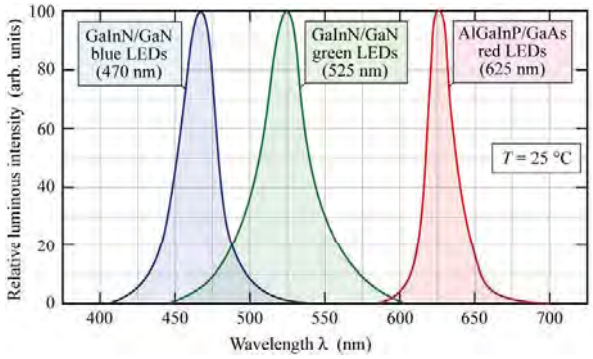

Fig. 12.16. Typical emission spectrum of GaInN/GaN blue, GaInN/GaN green, and AlGaInP/GaAs red LEDs at room temperature (after Toyoda Gosei Corp., 2000).

Temperature dependence

- GaInN output power has weak dependence on temperature

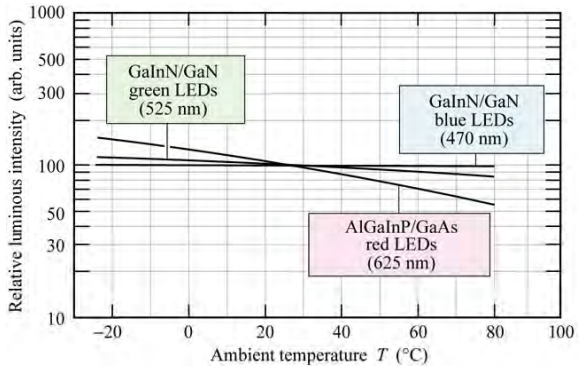

Fig. 12.18. Typical output intensity of GaInN/GaN blue, GaInN/GaN green, and AlGaInP/GaAs red LEDs versus ambient temperature (after Toyoda Gosei Corp., 2000).

Light output power (LOP) versus current

- AlGaInP is more mature than GaInN

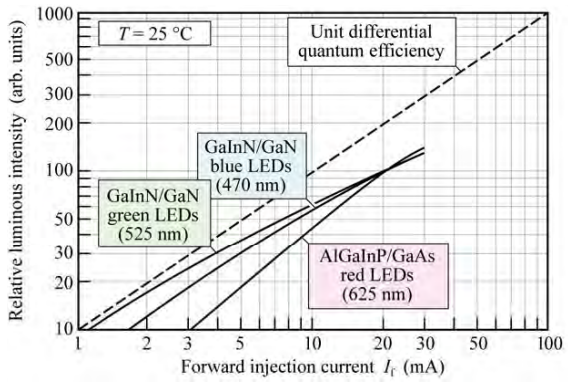

Fig. 12.17. Typical light output power vs. injection current of GaInN/GaN blue, GaInN/GaN green, and AlGaInP/GaAs red LEDs at room temperature (adopted from Toyoda Gosei Corp., 2000).

Electrical characteristics of high-brightness LEDs

- AlGaInP is more mature than GaInN

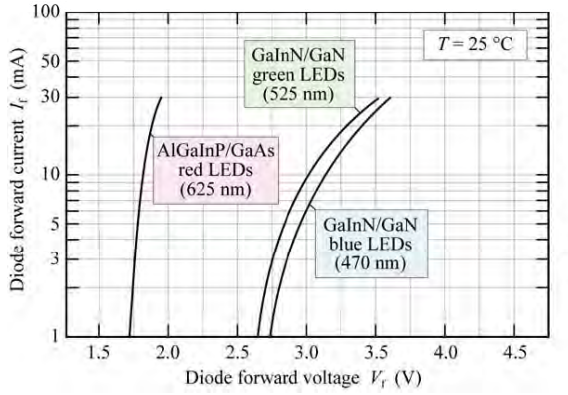

Fig. 12.19. Typical forward current–voltage (I–V) characteristic of GaInN/GaN blue, GaInN/GaN green, and AlGaInP/GaAs red LEDs at room temperature (after Toyoda Gosei Corporation, 2000).

Forward voltage versus temperature

- Forward voltage decreases with temperature
- Forward voltage can be used for junction temperature measurements

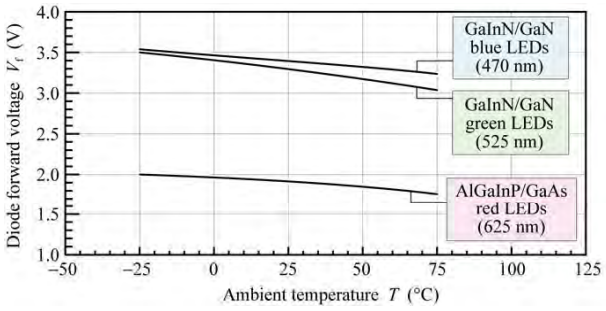

Fig. 12.20. Typical diode forward voltage at a current of 30 mA of GaInN/GaN blue, GaInN/GaN green, and AlGaInP/GaAs red LEDs versus temperature (after Toyoda Gosei Corp., 2000).

Solid-state lighting

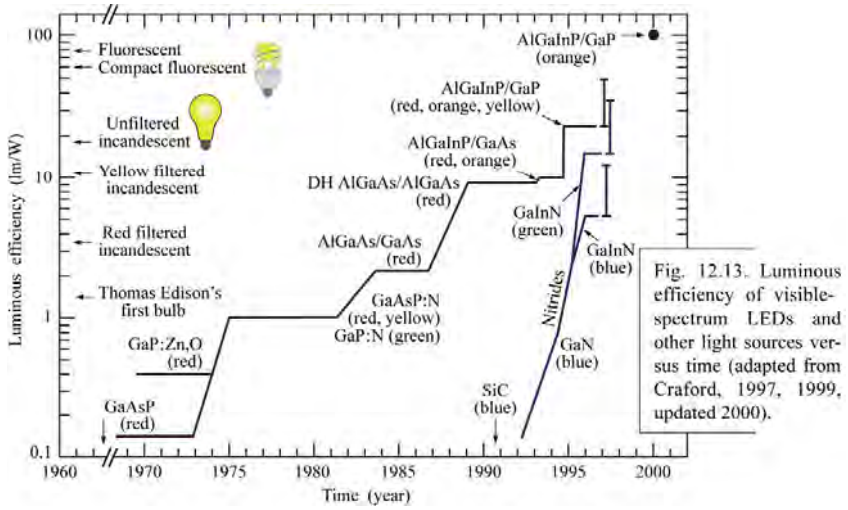

Fig. 12.13. Luminous efficiency of visible-spectrum LEDs and other light sources versus time (adapted from Craford, 1997, 1999, updated 2000).

- Strong progress over last decades; Update for white LEDs:
  - Large LED chip: ***2007***: 100 lm/W; ***2009***: 150 lm/W (at 350 mA, major companies)
  - Small LED chip: ***2009***: 249 lm/W (at 20 mA, device made by Nichia)

Comparison – Efficiency of LEDs versus other light sources

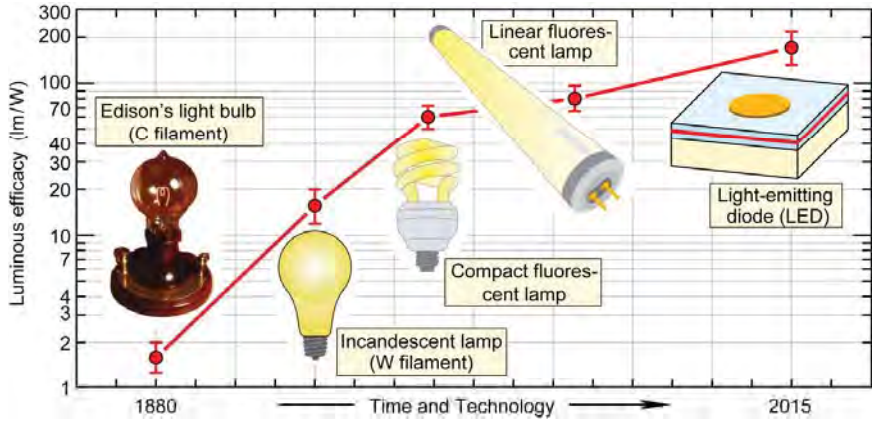

- Luminous efficacy of LEDs, to be attained by 2015, is based on the expectation that LEDs will be able to attain 50% to 70% of the theoretical maximum. The theoretical maximum of the luminous efficacy is 300 lm/W.

Comparison across spectrum

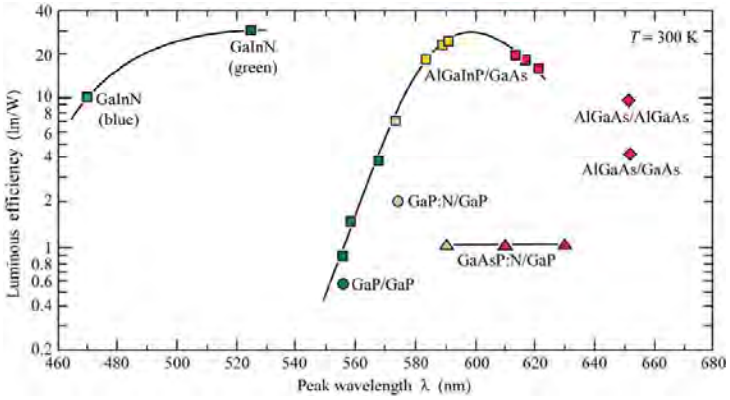

Fig. 12.14. Overview of luminous efficiency of visible LEDs made from the phosphide, arsenide, and nitride material system (adapted from United Epitaxy Corporation, 1999; updated 2000).

Lack of efficient LEDs at 550 nm is sometimes referred to as the "**green gap**"

The “green gap”

- Efficient LEDs, emitting at 550 nm, are, unfortunately, not yet available
- This fact is frequently referred to as the “Green Gap”

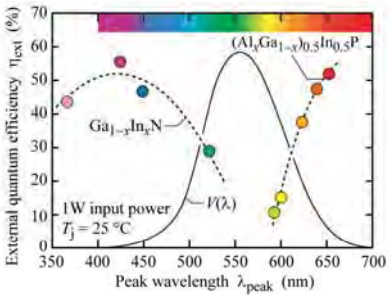

Fig. 20.3. External quantum efficiencies for high-power visible-spectrum LEDs made from the nitride and phosphide material system. $V(\lambda)$ is the luminous eye response curve of the CIE. The dashed lines are guides to the eye. (after Krames *et al.*, 2007).

Comparison: Light bulb versus LED

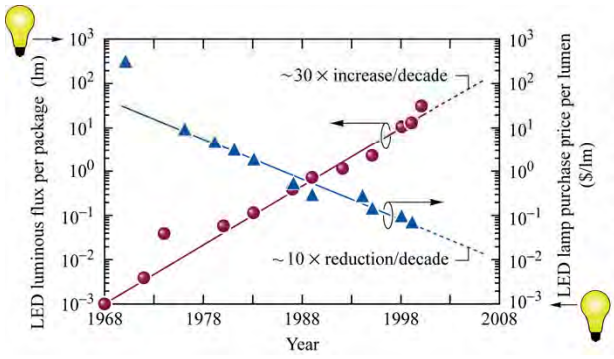

Fig. 12.15. LED luminous flux per package and LED lamp purchase price per lumen versus year. Also shown are the values for a 60 W incandescent tungsten-filament light bulb with a luminous efficiency of ~17 lm/W and a luminous flux of 1000 lm with an approximate price of 1.00 US$ (after Krames *et al.*, 2000).

- Approximate luminous flux of 60 W incandescent bulb: 1000 lm
- Approximate price of 60 W bulb: 1.00 $
- Incandescent bulb: 10^{-3} $/lm
- LEDs need a more than 10 × improvement in ***luminous flux*** and ***price per lumen***

Human vision

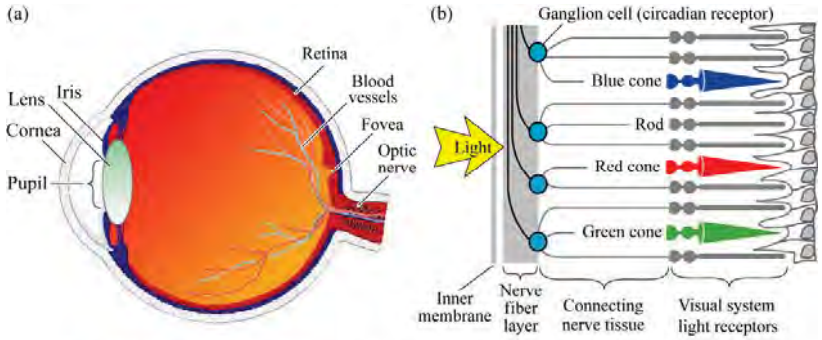

Fig. 16.1. (a) Cross section through a human eye. (b) Schematic view of the retina including rod and cone light receptors (adapted from Encyclopedia Britannica, 1994).

- **Cones**: Provide color sensitivity
- **Rods**: Color-insensitive
- Color perception depends on light level
- Scotopic vision regime: Low-light-level-vision regime
- Photopic vision regime: High-light-level-vision regime

Spectral sensitivity of rods and cones

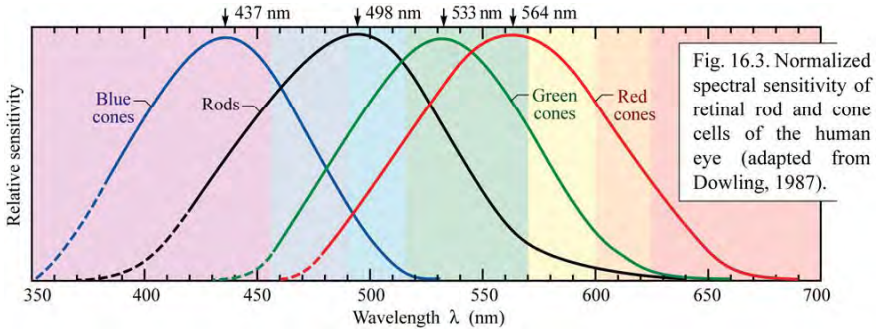

Fig. 16.3. Normalized spectral sensitivity of retinal rod and cone cells of the human eye (adapted from Dowling, 1987).

- Approximate spectral sensitivity
- There are radiometric units (W, W/m^2, etc.)
- There are photometric units (lm, cd, lux, etc.)

Photopic and scotopic vision regime

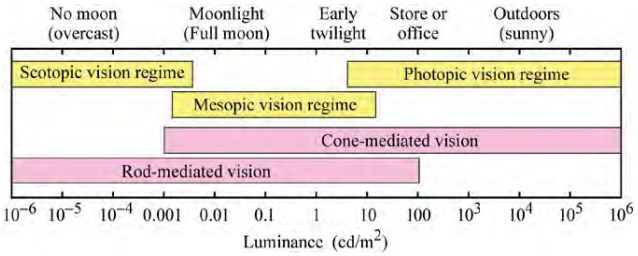

Fig. 16.2. Approximate ranges of vision regimes and receptor regimes (after Osram Sylvania, 2000).

Photopic vision regime = Daytime vision with full color perception
Scotopic vision regime = Nighttime vision with reduced color perception

There are several standards:

Photopic:
- CIE 1931, CIE 1978

Scotopic:
- CIE 1951


Photopic vision regime


Scotopic vision regime

History of photometric units

- Photograph shows **plumber's candle**
- A plumber's candle emits a **luminous intensity** of 1 candela (cd). The cd is historical origin of all photometric units.

- **First definition** (now obsolete): **The luminous intensity of a standardized candle is 1 cd**.
- **Second definition** (now obsolete): **1 cm^2 of platinum (Pt) at 1042 K (temperature of solidification) has a luminous intensity of 20.17 cd**.
- **Third definition** (current): **A monochromatic light source emitting an optical power of (1/683) Watt at 555 nm into the solid angle of 1 steradian (sr) has a luminous intensity of 1 cd**.
- *Candlepower* and *candle* are obsolete units. *Candlepower* and *candle* measure luminous intensity and are approximately equal to one cd.

Luminous flux, illuminance, and luminance

- **luminous flux**: A light source with a luminous intensity of 1 cd emits a luminous flux of 1 lm into a solid angle of one steradian
  - An isotropic light source with a luminous intensity of 1 cd emits a total luminous flux of 4π lm = 12.56 lm
- **Illuminance**: If a 1 m^2 surface receives a luminous flux of 1 lm, then the illuminance of the surface is 1 lux
  - Example: Moonlight 1 lux; reading light 10^2 – 10^3 lux; surgery light 10^4 lux; direct sunlight 10^5 lux
- **Luminance** is the luminous intensity emitted per unit area of a light source. Luminance is a figure of merit for displays. Typical displays have a luminance of 100 – 500 cd/m^2
- **Luminous efficacy of radiation** is the relative eye sensitivity of the human eye. At 555 nm, the relative eye sensitivity is 683 lm / W

Eye sensitivity function and luminous efficacy

- Visible wavelength range: 400 – 720 nm

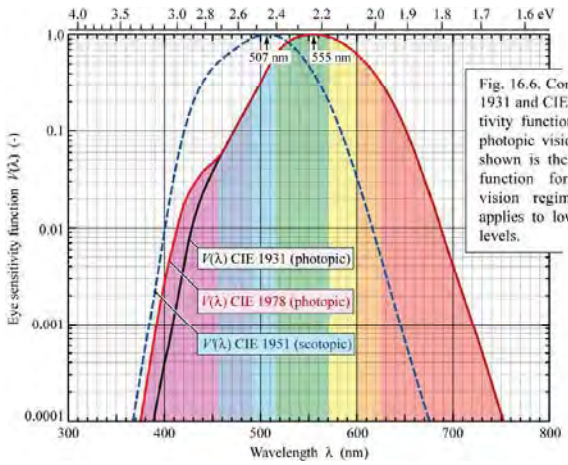

Fig. 16.6. Comparison of CIE 1931 and CIE 1978 eye sensitivity functions $V(\lambda)$ for the photopic vision regime. Also shown is the eye sensitivity function for the scotopic vision regime, $V'(\lambda)$, that applies to low ambient light levels.

- **Definition of lumen**: Green light (555 nm) with power 1 W of has luminous flux 683 lm
- **Efficacy of radiation** gives number of lumens per optical Watt
- Amongst LEDs with same output power, green LEDs are brightest

Luminous flux and efficiency

Luminous flux (Unit: lm)

$$\Phi_{\text{lum}} = 683 \frac{\text{lm}}{\text{W}} \int_{\lambda} V(\lambda)\, P(\lambda)\, \mathrm{d}\lambda$$

Luminous efficacy of radiation (Unit: lm / W)

$$\text{Luminous efficacy} = \Phi_{\text{lum}} / P = \left(683 \frac{\text{lm}}{\text{W}} \int_{\lambda} V(\lambda)\, P(\lambda)\, \mathrm{d}\lambda \right) \Big/ \left(\int_{\lambda} P(\lambda)\, \mathrm{d}\lambda \right)$$

Luminous efficacy of the source (Unit: lm / W)

$$\text{Luminous efficiency} = \Phi_{\text{lum}} / (IV)$$

Caution: Luminous "efficacy" and "efficiency" is being used in literature

Colorimetry and color matching functions

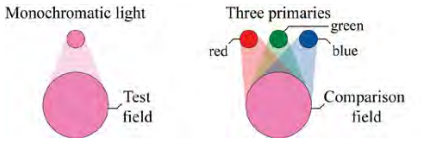

Fig. 17.1. Principle of color matching: A monochromatic test light (imaged on the "test field") is color-matched by mixing three adjustable primary lights, red, green, and blue (imaged on the "comparison field").

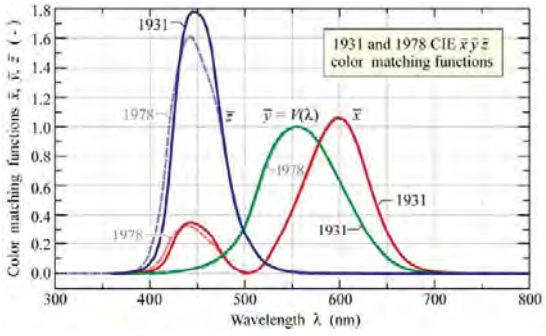

Fig. 17.2. CIE (1931) and CIE (1978) $\bar{x}\bar{y}\bar{z}$ color-matching functions. The $\bar{y}$ color-matching function is identical to the eye sensitivity function $V(\lambda)$. Note that the CIE 1931 color-matching functions are the currently valid official standard in the United States.

- Color matching functions are similar to the spectral sensitivity of the cones
- Caution: There are different standards for the color matching functions

Color matching functions and chromaticity

$$X = \int_\lambda \bar{x}(\lambda)\, P(\lambda)\, d\lambda$$

$$Y = \int_\lambda \bar{y}(\lambda)\, P(\lambda)\, d\lambda$$

$$Z = \int_\lambda \bar{z}(\lambda)\, P(\lambda)\, d\lambda$$

X, *Y*, and *Z* are ***tristimulus values***

Chromaticity diagram and ***chromaticity coordinates*** *x*, *y*

$$x = \frac{X}{X+Y+Z} \qquad y = \frac{Y}{X+Y+Z}$$

z chromaticity coordinate not needed, since $x + y + z = 1$

Uniform chromaticity coordinates *u*, *v* and *u'*, *v'*

x, *y* and *u'*, *v'* chromaticity diagram

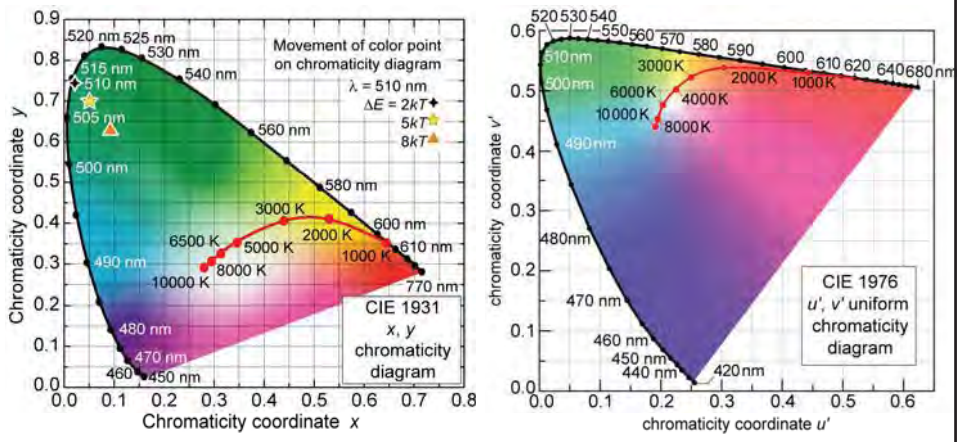

- Chromaticity diagrams allow us to ***quantify color (i.e. introduce a color metrics or colorimetry)***
- Planckian radiator
- Color temperature

MacAdam ellipses

x, y diagram

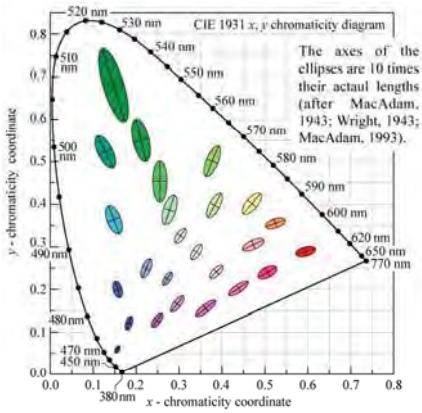

u', v' diagram

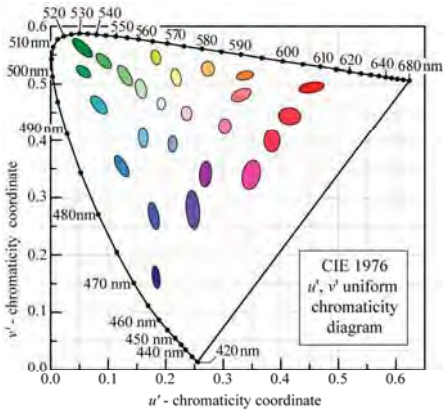

- Color differences cannot be discerned with in the MacAdam ellipses
- Axes of MacAdam ellipses are shown 10 times longer than they are
- Humans can discern about 50 000 different colors

Color purity and dominant wavelength

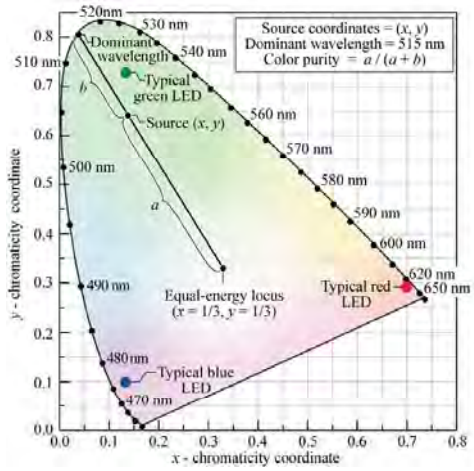

Fig. 17.9. Chromaticity diagram showing the determination of the *dominant wavelength* and *color purity* of a light source with chromaticity coordinates (x, y) using the equal-energy locus $(x = 1/3, y = 1/3)$ as the white-light reference. Also shown are typical locations of blue, green, and red LEDs.

Caution: Peak wavelength and dominant wavelength can be different.

Peak wavelength is a quantity used in physics and optics.

Dominant wavelength is used by in human vision.

LEDs in the chromaticity diagram

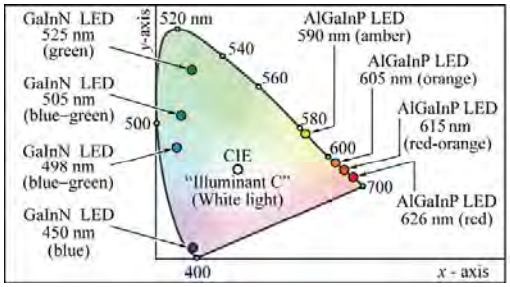

Fig. 17.10. Location of LED light emission on the chromaticity diagram (adapted from Schubert and Miller, 1999).

- **Note**:
- Red and blue LEDs are near perimeter of chromaticity diagram
- Green LEDs are not at perimeter but are shifted towards center
- Color purity and color saturation

Saturated color — Unsaturated color

White illuminant – the solar spectrum

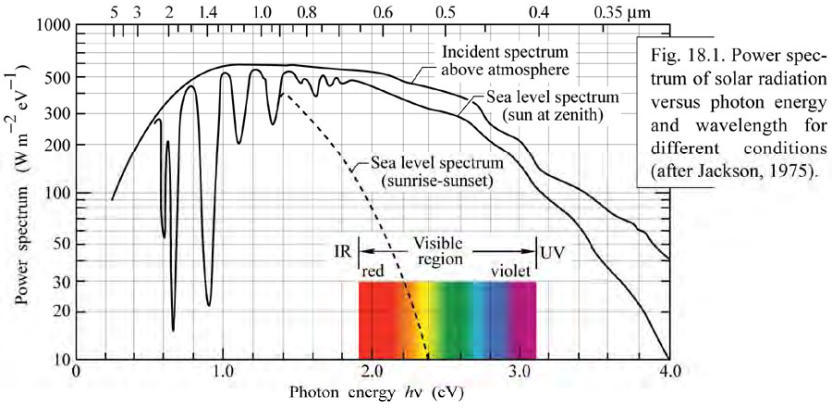

Fig. 18.1. Power spectrum of solar radiation versus photon energy and wavelength for different conditions (after Jackson, 1975).

- ***Note***: There are many ways to create white light
- Sunlight is not an efficient way to create white light. Why?

Planckian spectrum or black-body radiation spectrum

- A black body has no emission or reflection spectrum and thus no color
- Black-body radiation is ***heat glow*** or ***incandescence***
- Heat glow is a common phenomena

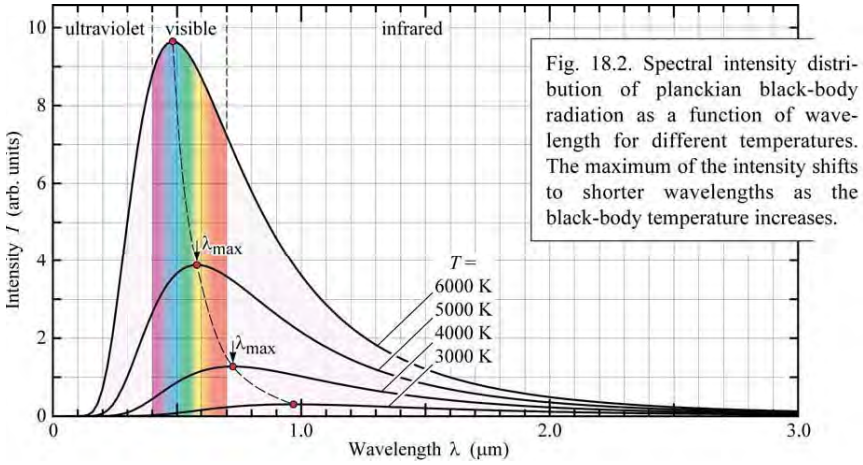

Fig. 18.2. Spectral intensity distribution of planckian black-body radiation as a function of wavelength for different temperatures. The maximum of the intensity shifts to shorter wavelengths as the black-body temperature increases.

Color temperature

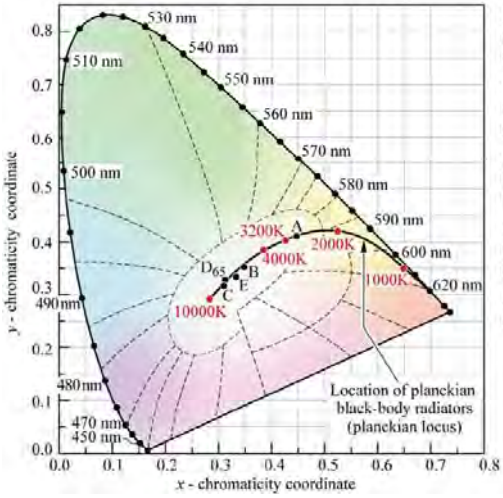

Illuminant A
(x, y) = (0.4476, 0.4074)
(Incandescent source, T = 2856 K)

Illuminant B
(x, y) = (0.3484, 0.3516)
(Direct sunlight, T = 4870 K)

Illuminant C
(x, y) = (0.3101, 0.3162)
(Overcast source, T = 6770 K)

Illuminant D_{65}
(x, y) = (0.3128, 0.3292)
(Daylight, T = 6500 K)

Illuminant E (equal-energy point)
(x, y) = (0.3333, 0.3333)

Fig. 18.3. Chromaticity diagram showing planckian locus, the standardized white illuminants A, B, C, D_{65}, and E, and their color temperatures (after CIE, 1978).

- ***Planckian*** spectrum or ***black-body radiation*** spectrum
- As temperature increases, objects sequentially glow in the red, orange, yellow, and white

Color mixing and color rendition

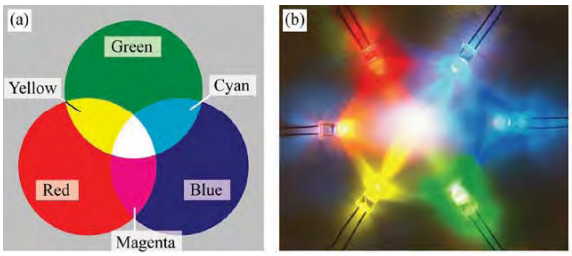

Fig. 19.1. (a) Schematic of additive color mixing of three primary colors. (b) Additive color mixing using LEDs.

- RGB color mixing
- Color gamut
- Gamut size increases with the number of light sources

Color mixing

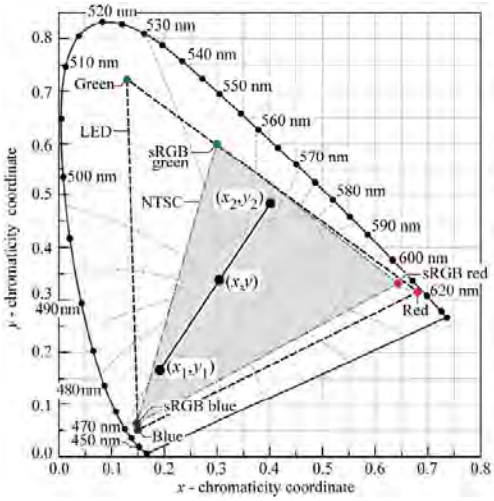

Fig. 19.2. Principle of color mixing illustrated with two light sources with chromaticity coordinates (x_1, y_1) and (x_2, y_2). The resulting color has the coordinates (x, y). Also shown is the triangular area of the chromaticity diagram (color gamut) accessible by additive mixing of a red, green, and blue LED. The locations of the red, green, and blue phosphors of the sRGB display standard ($x_r = 0.64$, $y_r = 0.33$, $x_g = 0.30$, $y_g = 0.60$, $x_b = 0.15$, $y_b = 0.06$) are also shown. The sRGB standard is similar to the NTSC standard.

- ***Color gamut***
- Gamut of Red-Green-Blue light source has triangular shape
- Area of gamut matters for displays, color printers, etc.

Color rendition

- A light source has ***color rendering capability***
- This is the capability to render the true colors of an object

- **Example**: ***False color rendering***
- What is the color of a yellow banana when illuminated with a red LED?
- What is the color of a green banana when illuminated with a yellow LED?

Example of color rendition

High CRI
illumination source

Low CRI
illumination source

Franz Marc “Blue Horse” (1911)

Color rendition

- The color rendering capability ***of a test light source*** is measured in terms of the ***color rendering index***
- Color rendering index of a high-quality ***reference light source*** is CRI = 100
- An incandescent light source with the same color temperature serves as the reference light source
- Eight color sample objects serve as test objects

Reflectivity of color sample objects

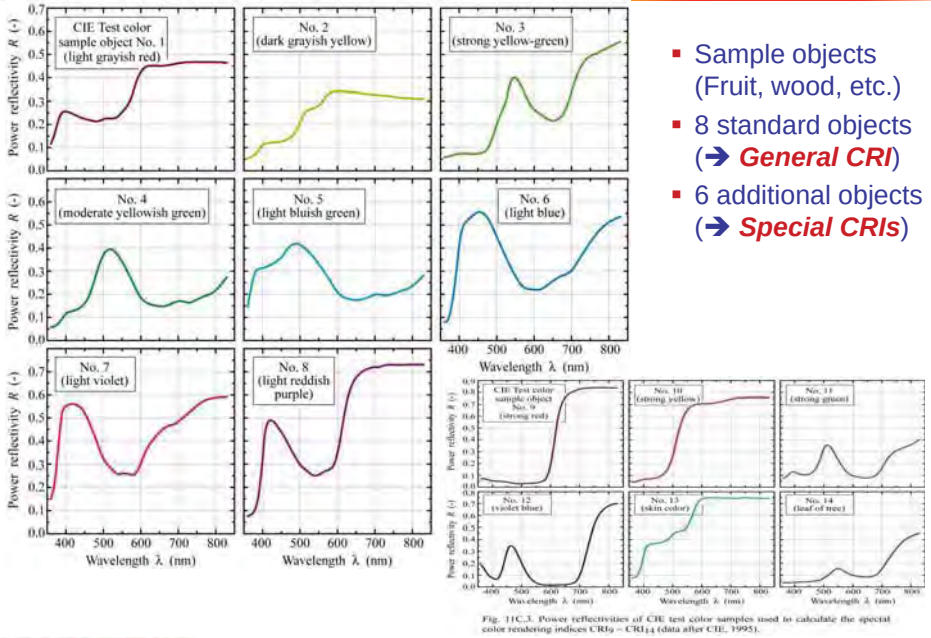

- Sample objects (Fruit, wood, etc.)
- 8 standard objects (➔ ***General CRI***)
- 6 additional objects (➔ ***Special CRIs***)

Color rendering index (CRI)

- The reference objects are illuminated with ***reference light source***. As a result, object will have a certain color.
- The reference objects are then illuminated with ***test light source***. As a result, object will have a certain, but different, color.
- The CRI is a measure of the sum of the differences in color.
- If color difference is zero, then *CRI* = 100
- If color difference is > zero, then *CRI* < 100
- Some applications require high and very high CRI. Examples?
- Some applications do not require a high CRI. Examples?
- For some applications, CRI is irrelevant. Examples?
- ***Caution***: CRI depends on the selection of the reference light source. Recommended for reference light source: Planckian radiator.

Color rendering

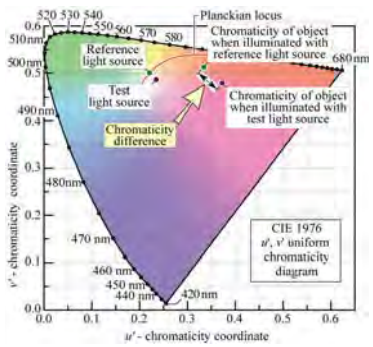

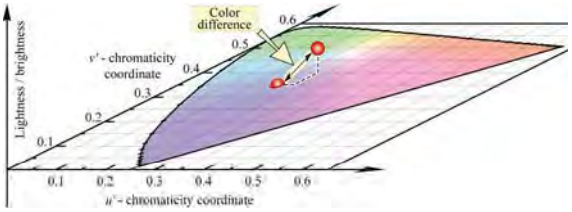

- CIE = Commission Internationale de L'Éclairage = International Commission on Illumination (Vienna, Austria)

- CIE color definition: **Color = Brightness, hue, and saturation**
- Color rendering index: $CRI = 100 - \Sigma_{i=1...8} \Delta E_i^*$
- ΔE_i^* depends also on color change and on luminance (brightness) change of object!
- Further complication: Chromatic adaptation and adaptive color shift.
- CRI is a very good metric – but not an ideal one!

Color render index examples

Light source	*Color rendering index*
Sunlight	100
Quartz halogen W filament light	100
W filament incandescent light	100
Fluorescent light	60 – 85
Phosphor-based white LEDs	60 – 90
Trichromatic white light LEDs	60 – 90
Hg vapor light coated with phosphor	50
Na vapor light	40
Hg vapor light	20
Dichromatic white light LEDs	10 – 60
Green monochromatic light	– 50

Table: Color rendering indices (CRI) of different light sources.

- CRI > 85 suitable for most (even most demanding) applications

White light emitters based on LEDs

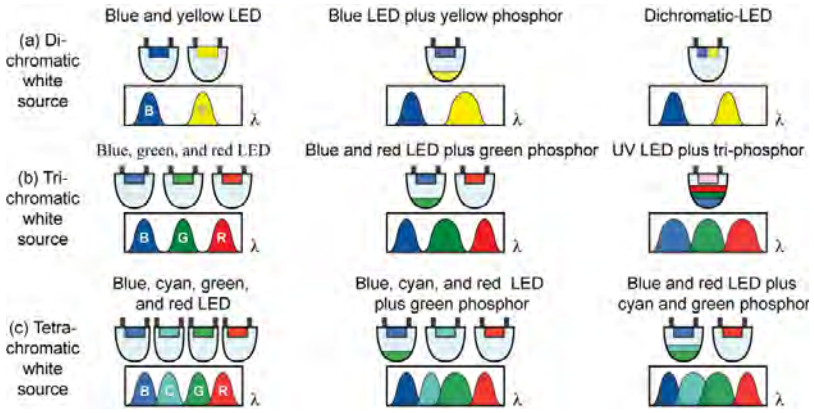

- Di-chromatic with phosphor: Commercial success but limited color rendering ability (CRI < 80)
- Phosphor-based approaches: Excellent color stability
- Phosphor-based approaches: *Stokes-shift* energy loss unavoidable
- Tri-chromatic LED-based approaches

Simplest approach: Dichromatic sources

Blue and yellow LED

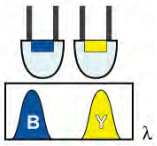

Fundamentally the most efficient way to create white light

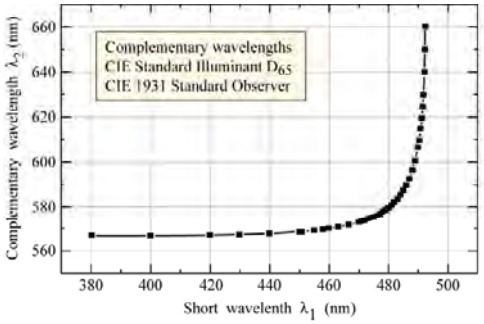

Fig. 20.2. Monochromatic complementary wavelengths resulting in the perception of white light at a certain power ratio (after Wyszecki and Stiles, 1982).

- Two complementary wavelengths give white light
- Example: Blue and yellow

Luminous efficacy of dichromatic light sources

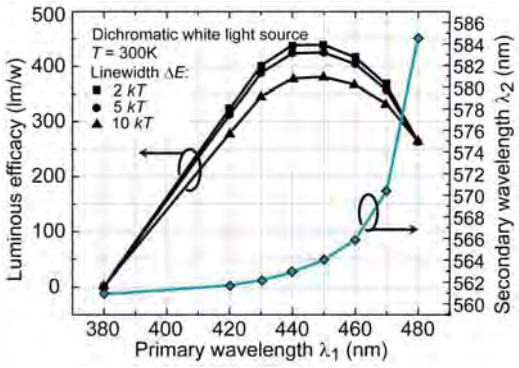

- Di-chromatic source is most efficient way to create white light outstanding
- Luminous efficacy > 400 lm/W for narrow emission lines
- However, CRI is low ➔ unsuitable for illumination applications
- Great display device (e.g. pedestrian traffic signal, display, etc.)
- There is a fundamental trade-off between CRI and luminous efficacy

Converters

- There are different types of converters: Dyes, polymers, phosphors, and semiconductors
- ***Phosphor*** converters are most common type of converter
- Ce-doped YAG (yttrium aluminum garnet) is a common type of converter
- Phosphor-based white light emitters are very stable (no temperature dependence)
- Semiconductors and dyes have been used as converters but are not very common

Wavelength converter materials – phosphors

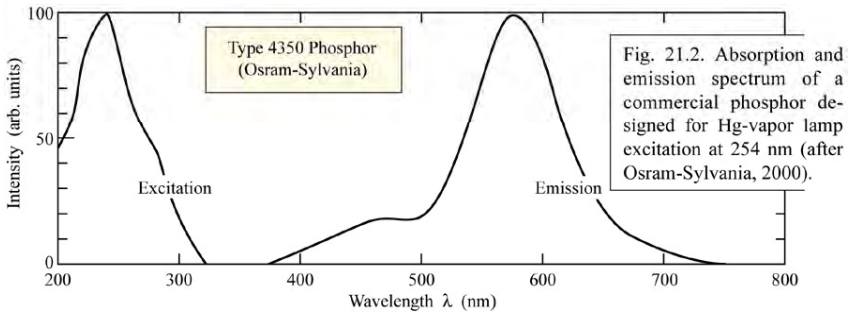

Fig. 21.2. Absorption and emission spectrum of a commercial phosphor designed for Hg-vapor lamp excitation at 254 nm (after Osram-Sylvania, 2000).

- This shows a typical phosphor used in a fluorescent tube
- Hg-lamp excitation at 200 – 250 nm
- Typical LED excitation is at ***460 nm*** for typical white LEDs consisting of blue LED and yellow posphor

Wavelength converter materials – dyes

- Long term stability?

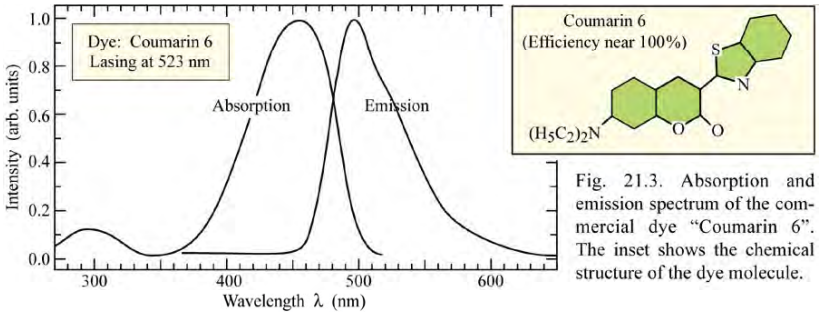

Fig. 21.3. Absorption and emission spectrum of the commercial dye "Coumarin 6". The inset shows the chemical structure of the dye molecule.

Wavelength converter materials – semiconductors

- Semiconductors are a possibility but not commonly used

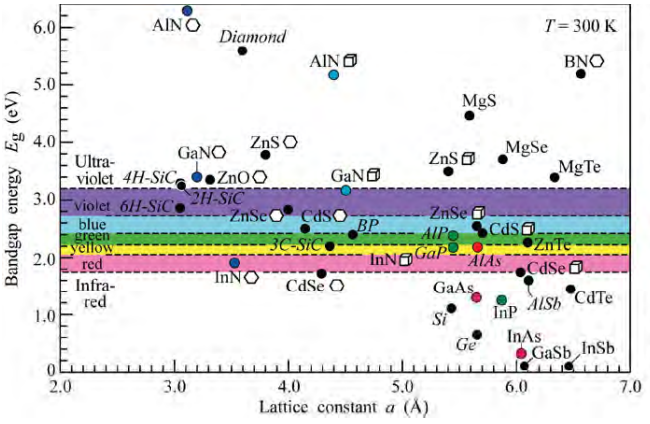

"*Italics*" = indirect gap
"Roman" = direct gap
⬡ hexagonal structure
⧈ cubic structure

Fig. 21.4. Room-temperature bandgap energy versus lattice constant of common elemental and binary compound semiconductors.

White LEDs based on phosphor converters

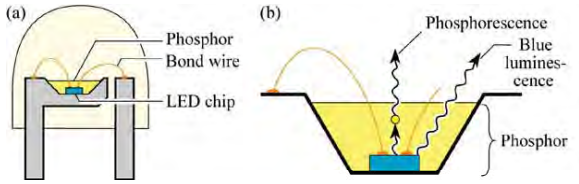

Fig. 21.7. (a) Structure of white LED lamp consisting of a GaInN blue LED chip and a phosphor. (b) Wavelength-converting phosphorescence and blue luminescence (after Nakamura and Fasol, 1997).

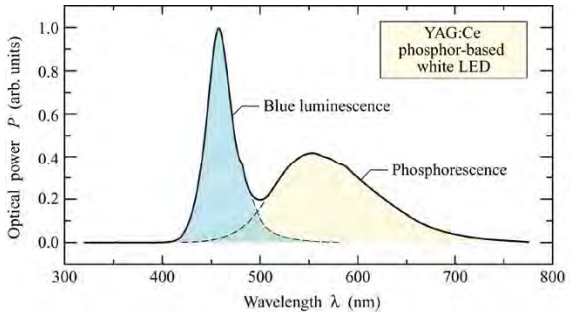

Fig. 21.8. Emission spectrum of a phophor-based white LED manufactured by Nichia Corporation (Anan, Tokushima, Japan).

First commercial white LED by Nichia Corporation (Japan)

Efficiency of white light source based on LEDs

- Efficiency of white light source based blue LED and yellow phosphor

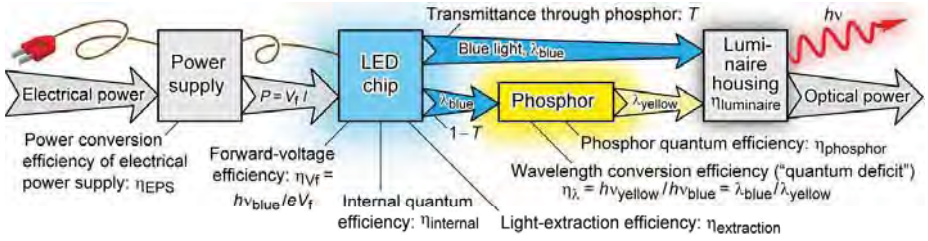

Formula for efficiency of white light source based on LEDs

$$\eta = \eta_{EPS} \times \left[(\eta_{Vf}\, \eta_{internal}\, \eta_{extraction})\, T + (\eta_{Vf}\, \eta_{internal}\, \eta_{extraction})\, (1-T)\, \eta_{phosphor}\, \eta_{\lambda} \right] \times \eta_{luminaire}$$

η	is the overall efficiency of white LED
η_{EPS}	is the efficiency of the electrical power supply which can be as high as 100%. In AC-driven scenarios, η_{EPS} = 100%. In DC scenarios, η_{EPS} can be greater than 90%.
η_{Vf}	is the electrical forward-voltage efficiency of the LED chip. It is $\eta_{Vf} = h\,\nu_{blue} / (e\,V_f)$. Ideally, the forward energy ($e\,V_f$) would be equal to the photon energy, so that η_{Vf} = 100%. However, for many current LED structures, V_f exceed this target value, particularly at high currents, where the series resistance loss, IR^2, is large. Thus, there is room for significant improvement of η_{Vf}.
$\eta_{internal}$	is the internal quantum efficiency of the LED chip. For most LED chips, there is room for significant improvement of $\eta_{internal}$.
$\eta_{extraction}$	is the quantum efficiency for light to be extracted out of the LED chip and housing. For most LED chips, there is room for significant improvement of $\eta_{extraction}$.
T	is the fraction of light transmitted through the yellow phosphor.
$\eta_{phosphor}$	is the quantum efficiency of the phosphor material, i.e. the ratio of photons emitted by the phosphor divided by photons absorbed by the phosphor. For optimized structures, $\eta_{phosphor}$ can be high, greater than 90%. However, for non-optimized structures, such as structures having non-uniform phosphors distribution, $\eta_{phosphor}$ can less than 50%.
η_{λ}	is the wavelength conversion efficiency, limited by the energy loss when converting one blue photon into one yellow photon ("quantum deficit"). It is $\eta_{\lambda} = h\nu_{yellow} / h\nu_{blue} = \lambda_{blue} / \lambda_{yellow}$. This loss is unavoidable in LEDs employing a phosphor and is particularly high when UV excitation is used. Note that the quantum deficit is particularly high for conventional fluorescent sources that are based on Hg discharge lamps which emit in the deep UV at about 250 nm.
$\eta_{luminaire}$	is the efficiency of the luminaire housing surrounding the LED. Depending on the application, not every application requires a luminaire housing. Therefore, the luminaire efficiency can be as high as 100%.

White LEDs based on phosphor converters

- Enhance color rendering by broadening spectrum

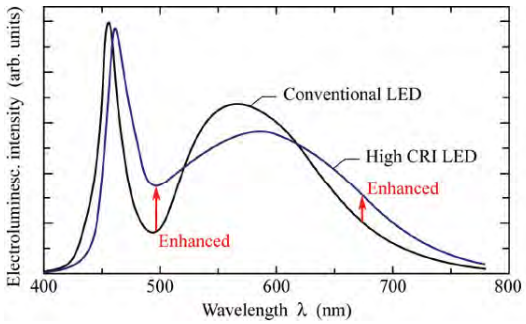

Fig. 21.10. Electroluminescence spectrum of conventional white LED and of high-color-rendering-index white LED. The high CRI results from the broader emission spectrum and the reduction of the notch in the spectrum (after Narukawa, 2004).

White LEDs based on phosphor converters

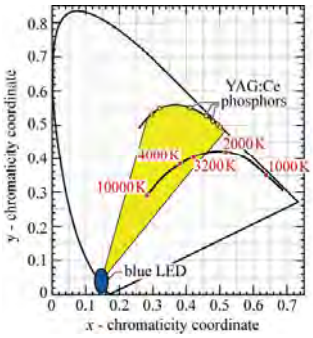

Fig. 21.6. Chromaticity points of YAG:Ce phosphor, and the general area (shaded) accessible to white emitters consisting of a blue LED and YAG:Ce phosphor (adapted from Nakamura and Fasol, 1997). Also shown is the planckian locus with color temperatures.

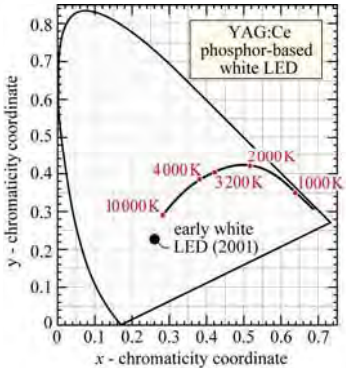

Early white LEDs can had a bluish tint and high color temperature.

Current white LEDs can have low as well as high color temperatures .

Proximate and remote phosphor distributions

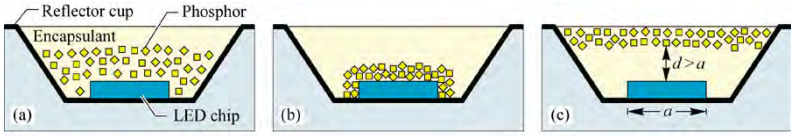

Fig. 21.11. (a) Proximate phosphor distribution, (b) proximate conformal phosphor distribution, and (c) remote phosphor distribution in which phosphor and chip are separated by at least one times the lateral dimension of the chip (after Kim *et al.*, 2005).

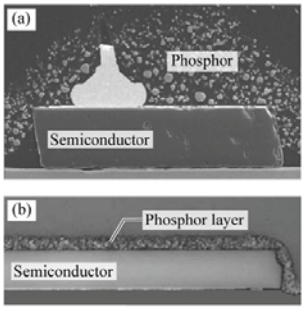

Fig. 21.12. Phosphor distributions in white LEDs: (a) Proximate phosphor distribution. (b) Proximate conformal phosphor distribution. (c) Remote phosphor distribution ((a) and (b) adapted from Goetz, 2003; (c) after Kim *et al.*, 2005).

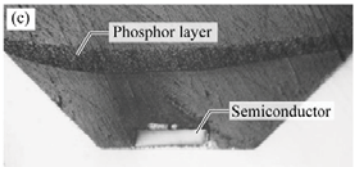

White LEDs based on semiconductor converters

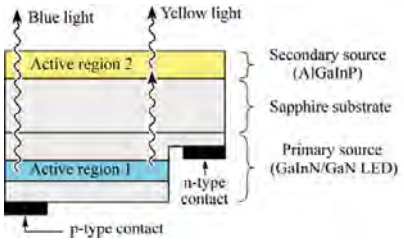

Fig. 21.13. Schematic structure of a photon-recycling semiconductor LED with one current-injected active region (Active region 1) and one optically excited active region (Active region 2) (after Guo *et al.*, 1999).

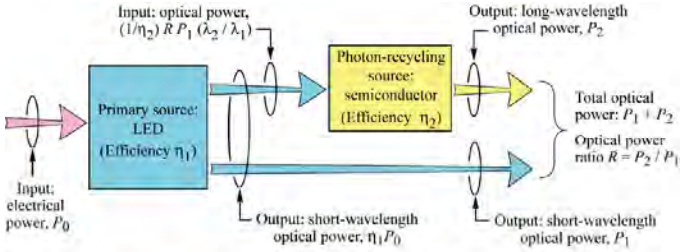

Fig. 21.14. Photon-recycling semiconductor LED power budget with electrical input power P_0 and optical output power P_1 and P_2.

Spectrum of PRS-LED

- This is an all-semiconductor white LED

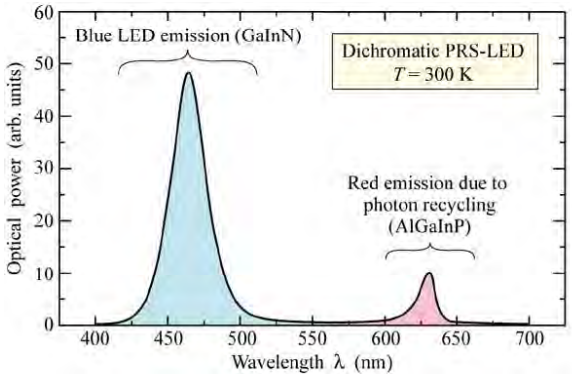

Fig. 21.17. Emission spectrum of dichromatic PRS-LED with current-injected GaInN blue LED primary source and AlGaInP photon recycling wafer (secondary source) emitting in the red (after Guo *et al.*, 2000).

Multi-LED white light sources

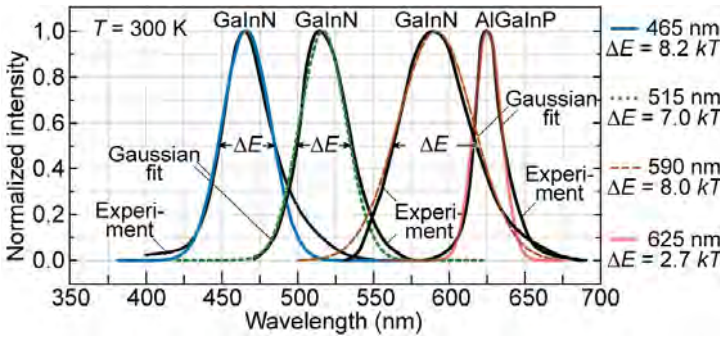

- Experimental LED emission linewidth ranges between 2.7 *kT* and 8.2 *kT*
- Much broader than predicted value of 1.8 *kT*
- Difference due to *alloy broadening*
- Alloy broadening particularly strong for GaInN
- Alloy broadening helps color rendering

Analysis of tri-chromatic LED source

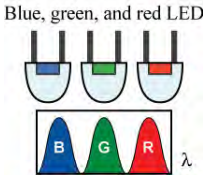

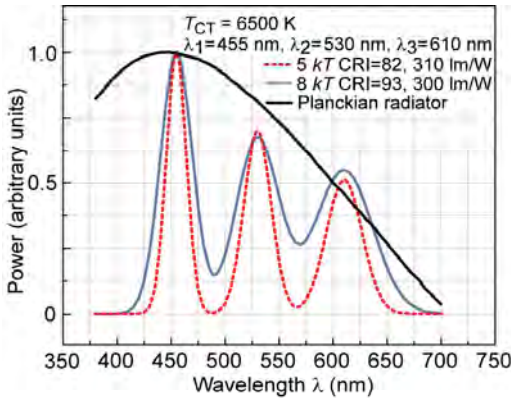

- Color temperature: 6500 K
- Comparison of tri-LED and 6500 K planckian radiator.
- Color temperature (T_C) of incandescent sources: 2800 K
- Spectral depressions are no significant problem due to the broad reflectivity features of real objects
- Spectrum can be designed
- Emission spectrum can be optimized

Demonstration of trichromatic source

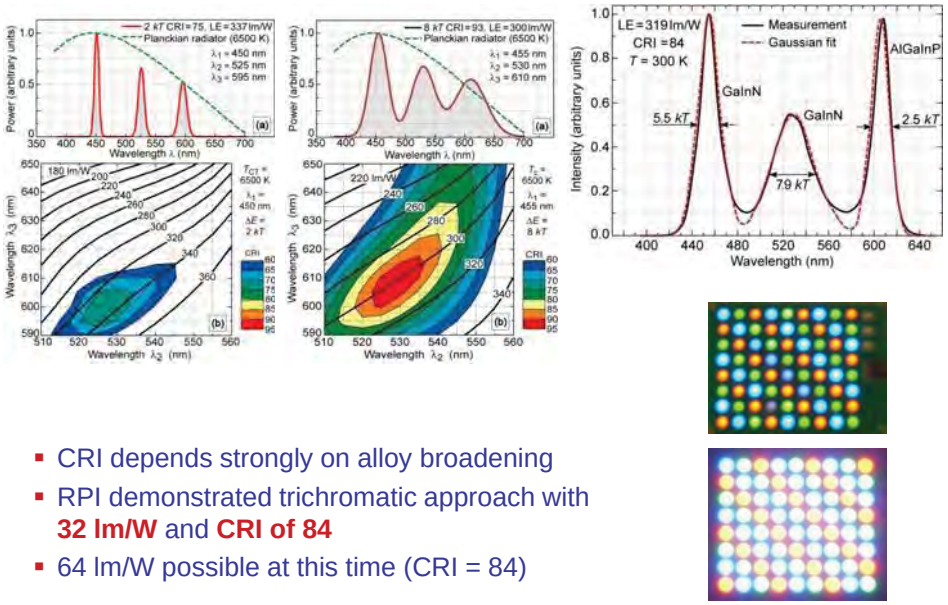

- CRI depends strongly on alloy broadening
- RPI demonstrated trichromatic approach with **32 lm/W** and **CRI of 84**
- 64 lm/W possible at this time (CRI = 84)

Luminous efficacy and CRI of tri-chromatic source

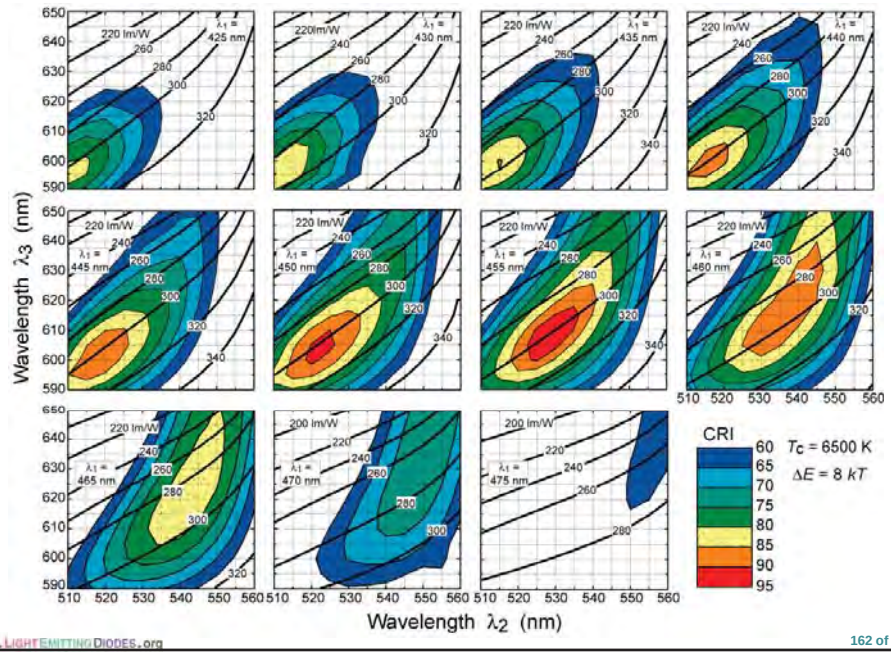

Tri-chromatic white LED sources

- All-semiconductor approaches to solid-state lighting provide highest luminous efficacy and potentially highest luminous efficiency
- CRI depends sensitively on source spectral width
- Tri-chromatic systems with $\Delta E = 8\ kT$:
- > 300 lm/W with CRI > 90, suitable for virtually all applications
- Tri-chromatic systems with $\Delta E = 5\ kT$:
- > 300 lm/W with CRI > 80, suitable for most applications
- ➔ Intentional emission-line broadening can be beneficial for CRI

Further information: *Light-Emitting Diodes*

Light-Emitting Diodes, second edition
ISBN: 0521865387
***Cambridge University Press, Cambridge UK*, 2006**

The second edition of this graduate textbook offers a comprehensive explanation of the technology and physics of LEDs such as infrared, visible-spectrum, ultraviolet, and white LEDs made from III-V semiconductors. Elementary properties such as electrical and optical characteristics are reviewed, followed by the analysis of advanced device structures. With nine additional chapters, the treatment of LEDs has been vastly expanded, including new material on device packaging, reflectors, UV LEDs, III-V nitride materials, solid-state sources for illumination applications, and junction temperature. Radiative and non-radiative recombination dynamics, methods for improving light extraction, high-efficiency and high-power device designs, white-light emitters with wavelength-converting phosphor materials, optical reflectors, and spontaneous recombination in resonant-cavity structures are discussed in detail. With exercises, solutions, and illustrative examples, this textbook will be of interest to scientists and engineers working on LEDs and graduate students in electrical engineering, applied physics, and materials science.